The Effect of Biochar Addition on Infiltration Rate and Soil Aggregation in the Lab

by

Brendan Benson

A thesis submitted to the Faculty of the University of Delaware in partial fulfillment of the requirements for the degree of Honors Degree in Environmental Engineering with Distinction

Spring 2021

The Effect of Biochar Addition on Soil Infiltration Rate and Soil Aggregation in the Lab

by

Brendan Benson

Approved: _____

Paul T. Imhoff, Ph.D
Professor in charge of thesis on behalf of the Advisory Committee

Approved: _____

Erik H. Ervin, Ph.D
Committee member from the Department of Department Name

Approved: _____

Earl Lee II, Ph.D
Committee member from the Board of Senior Thesis Readers

Approved: _____

Michael Chajes, Ph.D.
Dean, University Honors College

ACKNOWLEDGMENTS

I would like to first thank my research advisor, Paul Imhoff, for reaching out to me about the opportunity to continue the work that Reid Williams started. I appreciate our weekly meetings where Dr. Imhoff always answers my questions with patience. I would also like to thank Seyyed Ali Akbar Nakhli for answering my questions and discussing our research. Ali has always assisted in my understanding of the experiment.

With his consistent help in the lab, I would like to thank Marcus Bowser. Marcus was always happy to help and easy to work with.

Finally, I would like to thank Reid Williams for instructing me on how to perform the column experiments. Reid allowed my introduction to this project to be relatively stress-free with great training and instruction on what my role in this experiment was.

Thank you.

TABLE OF CONTENTS

LIST OF TABLES

LIST OF FIGURES

ABSTRACT

The continuation of biweekly wetting-drying cycles to twelve soil types from four states allowed for the effect of biochar-amendment to be more clearly observed. The hypothesis that biochar amendment would increase infiltration in most soils depending on soil mineralogy and texture was tested. Of the twelve soils tested, six showed biochar-amended soils having higher steady state percolation rates compared to soils without biochar, as seen in Figure 4.1. These soils include DE-1, DE-3, MD-1, MD-2, MD-3, and NC-2. These increases in infiltration will be beneficial to stormwater treatment. Biochar has proven to reduce soil swelling for all replicates compared to control soils. Soils with biochar also show lower area of surface cracks before each storm event compared to control soils. The relation between the effective hydraulic conductivity ratio of soils with biochar to soils without biochar and volume change in control soils was also identified. Biochar amendment is beneficial in reducing soil swelling and cracking for replicates.

Chapter 1

INTRODUCTION

1.1 Biochar Amendment

Biochar is a substance made by heating biomass with limited oxygen. It is applied to soil to sequester carbon and is meant to improve soil fertility and hydraulic function. Biochar has fused aromatic ring structures that are formed by pyrolysis. These structures are the reason behind the adsorption properties of biochar (Lehmann, 2015). Biochar has been added to soils along highways as a tool of stormwater management to increase stormwater infiltration. Dr. Imhoff and his team added biochar to soil beside a highway. They found that soil containing biochar reduced the average stormwater runoff volume by 84 percent, and the peak flow rate by 77 percent, compared to the control soils (Landers, 2018).

1.2 Soil Aggregation

Soil aggregation is a process that influences soil structure and water infiltration and flow rate through soils. Soil organic carbon creates regions of aggregation in soil caused by heterogeneity. Increased soil organic carbon is directly related to increased particulate organic matter. Microorganisms in the soil decompose particulate organic matter and produce polysaccharides. Polysaccharides act as binding agents that initiate aggregation (Bronick, 2005). Biochar is a form of particulate organic carbon, some of which is biodegradable and, therefore might enhance polysaccharide production. The presence of fungi in soil also improves its aggregation. Fungi binds particles together,

along with polysaccharides, and enmesh particles to form macroaggregates (Bronick, 2005). Soils containing biochar are also expected to contain greater fungi hyphae length. Finally, soil is comprised of mineral, water, air, and organic components (Mukherjee, 2013). Adding biochar increases the fraction of organic matter in the soil. The carbon-based compounds in biochar and soil bind to the minerals in the soil. This process is known as organo-mineral association. Organo-mineral association is believed to be the start of the soil aggregation process. Organo-mineral association, coupled with microbial effects of polysaccharides produced by bacteria and hyphae produced by fungi lead to stable soil aggregates being formed (Mukherjee, 2013).

1.3 Reid Williams' Experiments

Dr. Imhoff's recent undergraduate student, Reid Williams, collected roadway soils from Delaware, Maryland, North Carolina, and California. These soils cover a range of soil texture and soil organic matter contents and are representative of roadway soils in the US. The texture, percent clay, percent silt, and precent sand of these soils are shown in Table 1.1. He constructed columns using PVC and measured the infiltration rate of these soils that underwent biweekly storm events for 18 weeks, some with added biochar. The soil classification for biochar-amended soils in shown in Table 1.2. Figure 1.1 shows the USDA soil texture classes of each soil in percent by weight sand, silt, and clay. The soils from Delaware showed small increases in infiltration rate when biochar was added, consistent with independent laboratory and field experiments conducted by other students in Dr. Imhoff's group. However, these changes were much less than those that were observed in other laboratory and field experiments. Reid concluded that 18 weeks was not long enough to draw precise

conclusions. However, the reason that biochar amendment to Delaware soils did not result in the same large changes in infiltration rate observed in other laboratory experiments was not conclusively determined.

Table 1.1: Control soil texture information by mass.

State	Texture	Name	Coordinate	% Sand	% Silt	% Clay
Delaware	Sandy Loam	DE-SaL or DE-1	39.530149, -75.736402	7.60	32.5	59.9
Delaware	Silty Loam	DE-SiL or DE-2	39.668703, -75.739079	13.6	52.0	34.4
Delaware	Loam	DE-L or DE-3	39.390678, -75.747972	7.80	45.5	46.7
Maryland	Silty Loam	MD-SiL or MD-1	39.643594, -75.801403	14.0	60.8	25.3
Maryland	Sandy Loam	MD-SaL or MD-2	39.612722, -76.00388	6.7	47.3	46
Maryland	Silty Loam (higher organic matter)	MD-SiL-O or MD-3	39.636240, -75.957593	12.7	60.5	26.8
California	Loam	CA-L or CA-1	36.009600, -78.490866	8.30	41.3	50.4
California	Clay Loam	CA-CL or CA-2	35.957595, -78.265870	33.6	45.3	21.1
California	Sandy Loam	CA-SaL or CA-3	35.820282, -78.265870	9.70	21.7	68.8
North Carolina	Loam	NC-L or NC-1	38.597506, -121.766812	24.2	28.7	47.1
North Carolina	Sandy Loam	NC-SaL or NC-2	38.561389, -121.786044	14.5	27.3	58.2
North Carolina	Clay Loam	NC-CL or NC-3	38.489180, -121.804229	35.9	36	28.1

Table 1.2: Biochar-amended soil texture information by mass.

State	Texture	Name	% Sand	% Silt	% Clay
Delaware	Sandy Loam	DE-SaLBC or DE1-BC	7.28	31.51	61.21
Delaware	Silty Loam	DE-SiLBC or DE2-BC	13.04	50.25	36.71
Delaware	Loam	DE-LBC or DE3-BC	7.45	44.01	48.54
Maryland	Silty Loam	MD-SiLBC or MD1-BC	13.40	58.66	27.94
Maryland	Sandy Loam	MD-SaLBC or MD2-BC	6.43	45.76	47.81
Maryland	Silty Loam (higher organic matter)	MD-SiL-OBC or MD3-BC	12.23	58.38	29.39
California	Loam	CA-LBC or CA1-BC	8.00	39.94	52.05
California	Clay Loam	CA-CLBC or CA2-BC	32.26	43.77	23.97
California	Sandy Loam	CA-SaLBC or CA3-BC	9.36	21.10	69.54
North Carolina	Loam	NC-LBC or NC1-BC	23.25	27.87	48.88
North Carolina	Sandy Loam	NC-SaLBC or NC2-BC	13.95	26.52	59.53
North Carolina	Clay Loam	NC-CLBC or NC3-BC	34.42	34.91	30.66

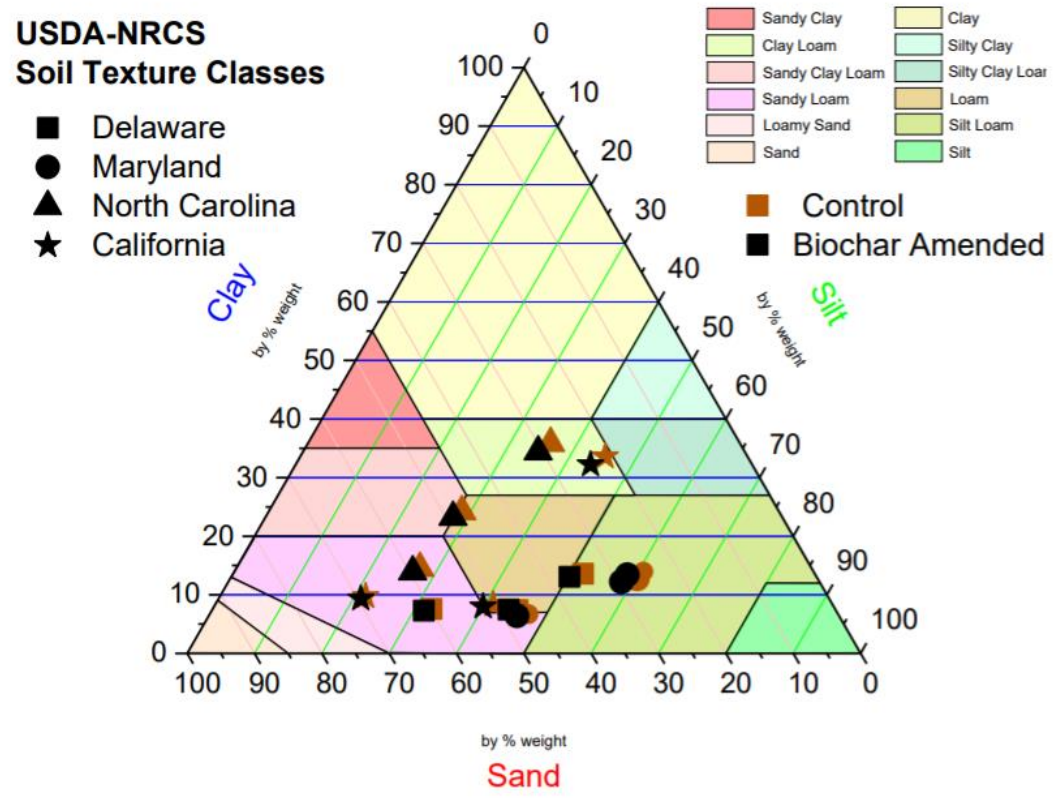

Figure 1.1: USDA Soil Texture Classes of control and biochar amended soils based on % sand, silt, and clay by mass (taken with permission from Reid, 2020).

1.4 Soil Cracking

Biochar has been seen to influence the nature of soils to affect the tendency of cracks to form. It is important to measure the effect of soil cracking on soil properties since soil cracking can significantly change the mobility of contaminants in soil, which effects the performance of biochar in remediation applications (Zhang, 2020). We must ensure that large cracks do not form throughout the soil volume in each column. These cracks may absorb large amounts of rainwater during routine wetting cycles, which can cause preferential flow and delay runoff initiation (Romkens, 2006).

The presence of preferential flow would cause increased variations in the steady state percolation rate in the experimental columns described below, so it must be confirmed that preferential flow is not occurring. X-Ray computed tomography can be used to quantity the three-dimensional soil structure, looking at cracking both qualitatively and quantitatively (Tang, 2019).

Chapter 2

GOALS OF RESEARCH

I was brought on to continue Reid Williams' work and expand upon it. Due to COVID-19, Reid had only been performing storm events from October 2019 to February 2020. The column experiments would be restarted and continued for a longer time, thus testing one hypothesis about the cause of less significant effect of biochar on Delaware soils – inadequate number of wetting-drying cycles. I continued performing the same storm events that Reid performed in the same biweekly cycle. I also completed additional measurements before and after each storm event, including quantifying cracking, soil volume, and volumetric water content. These measurements are intended to assess biochar's impact on soil cracking, soil swelling, and water retention.

Chapter 3

MATERIALS AND METHODS

3.1 Column Construction and Packing

Reid Williams constructed each column, prepared each soil for packing, and packed each column in Fall 2019. Three roadway soils from Delaware, Maryland, California, and North Carolina each were pretreated to a moisture content of 12-15% by mass. The soils were then ground up and placed in an oven at 105°C for 24 hours, where final moisture content was measured, and soils were sealed until the packing process. Dry soil mass was calculated using the final moisture content, and 4% biochar was added by dry mass. A 12-15% gravimetric moisture content was then achieved by adding water to the soil-biochar mixtures. Commercial biochar from Soil Reef LLC in Berwyn, PA was formed by pyrolyzing yellow pine at 550°C for 10 minutes and was dried and sealed in buckets until mixed with the soil. The particle size distribution for each soil was determined using ASTM standard D422 (ASTM D422 2007).

Next, 7.79 cm-diameter PVC piping was used to construct each column. Each column had a total volume of 477 cm^3. Two holes were drilled toward the top of each column on opposite sides. A plastic tube was glued to one of these holes to transfer runoff. Another hole was drilled at the bottom of each column to allow infiltrated water to drip out. Figure 3.1 shows the column setup. Figures E.1 and E.2 in Appendix E show the column dimensions in plan-view and elevation-view. Holes were also drilled on the sides of the column toward the bottom to equalize the pressure at the bottom of each column and to ensure that atmospheric pressure conditions were maintained at the bottom of each column. Soil was packed into each column using standard procedures. Three columns containing biochar and three columns without

biochar were packed for each soil type, totaling 72 columns. Columns were sealed after packing until all columns were ready to undergo their first storm event (Williams 2020).

Figure 3.1: Infiltration test setup for one column (taken with permission from Reid, 2020).

3.2 Stormwater

The same artificial stormwater Reid Williams used during storms 1-16 was used for all later storm events. The compounds shown in Table 3.1 were added to DI water and left to sit for 24 hours to achieve the desired properties of natural stormwater. The artificial stormwater solution was created in 22L quantities, so 19L of DI water was added initially. Then, 12.1g calcium chloride, 0.302g sodium phosphate, 0.267g sodium nitrate, and 0.168g ammonium chloride were mixed into the DI water. The pH was then measured and adjusted to the desired value of 7 using 5M HCl or 5M

NaOH. After the desired pH was reached, DI water was added for a total volume of 22L (Davis, 2003).

Table 3.1: Stormwater Concentrations used.

Parameter	**Value (mg/L, except pH)**	**Source**
pH	7.0	HCl or NaOH
Total dissolved solids	500	$CaCl_2$
Phosphorus	3 (as P)	Na_2HPO_4
Nitrate	2 (as N)	$NaNO_3$
Ammonium	2 (as N)	NH_4Cl

3.3 Artificial Stormwater Events

Each column underwent an artificial stormwater event roughly once every two weeks to mimic the wetting-drying cycle soils experience in nature. Three columns with biochar and three columns without biochar experienced storm events for all twelve soil types. Figure 3.1 shows the infiltration test setup for one column, with holes labeled A, B, and C. An inflow tube, at label A, was attached to the hole toward the top of each column, whose outlet rest at the center of the soil surface. A graduated cylinder was situated to collect the runoff from the soil surface that dripped from the tube attached to the front of each column, labeled B. Another graduated cylinder was situated beneath each column to collect percolated water, labeled C. Trypan blue dye was inserted into each graduated cylinder to ensure collected water was visible in a camera. The column setup for one storm event is shown below in Figure 3.2. Timed

photographs were taken during each storm event to observe the volume of water in each graduated cylinder throughout the duration of the storm event, whose values would be used in future measurements.

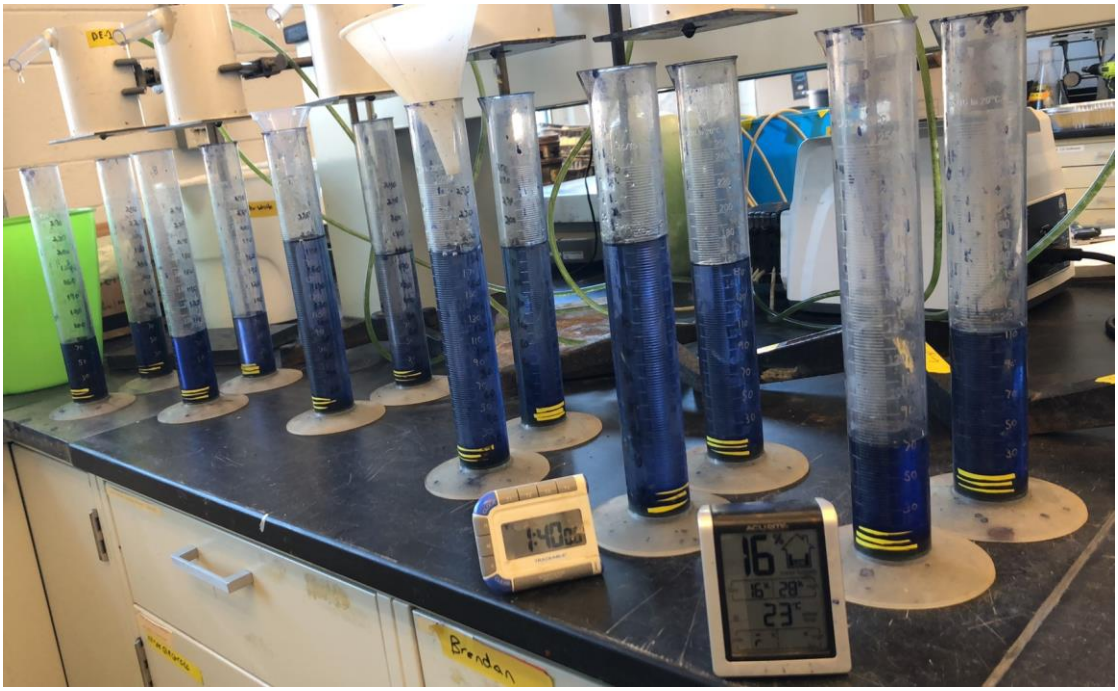

Figure 3.2: Infiltration test example. Storm 20 test of DE-1.

3.4 Steady-state percolation rate

The steady state percolation rate was calculated using the timed photographs taken during the storm event. The last quarter of the storm event duration was determined to be when the soils had reached steady state. The percolation rate at time *N* is quantified by the following equation:

$$Q_N = \frac{V_N - V_{N-1}}{T_N - T_{N-1}} \tag{3.1}$$

T is equal to the time after starting the storm event in minutes, *Q* is equal to the flow rate in mL/min, and *V* is equal to the volume of water collected in the graduated cylinder at time *N* in mL.

3.5 Soil volume

The volume of soil in each column was measured before and after each storm event. The diameter of soil in each column remained the same throughout the experiment. The soil height, however, increased or decreased from its initial value for all columns. The level of depression was measured for each soil by using a micrometer to measure the initial depth of soil from the top of the column. Five measurements were taken at the surface of each column, one toward the center of each quadrant and one at the middle of each column, shown in Figure 3.3. The average of these five measurements subtracted by the reference measurement resulted in an average level of depression value for each column. The level of depression was subtracted from the initial soil height, and the volume of soil was found using the soil diameter and the new soil height.

Figure 3.3: Location of level of depression measurements on column surface.

3.6 Soil Surface Cracking

Photographs of the soil surface of each column were taken before and after each storm event. These photos were opened in ImageJ (Java, Madison, Wisconsin) and cropped so the entire soil surface was visible. The dimensions of the photo were set in ImageJ by using the diameter of the soil surface, which was 7.79 cm for each column. Setting this dimension in ImageJ allowed for the total area of the photo to shown within the application. The maximum crack width was then measured for each column. The image was then converted to 8-bit to allow its threshold to be adjusted. The threshold was then adjusted accordingly so only the cracks were highlighted. The percentage of the image area was shown by ImageJ, and this value was multiplied by the area of the image to achieve the total area of cracking. The total area of cracking

was then divided by the area of the soil surface to find the percentage of the soil surface with cracks. This procedure was completed for photos taken before and immediately after each storm event.

3.7 Volumetric Water Content

The mass of each column was measured before and roughly forty-five minutes after shutting off the inflow pump. Measurements were taken at this time since most of the pore water in the columns had drained out after forty-five minutes. The gravimetric moisture content was calculated by dividing the mass of water in the soil by the dry soil mass. The mass of water in the soil was calculated by subtracting the mass of the empty column and the dry soil mass from the mass of the column and soil that was recorded. The dry soil mass and mass of the empty column were determined for each column by Reid Williams when he initially packed the columns. The initial gravimetric moisture content was calculated using the total mass before performing the wetting cycle, and the final gravimetric moisture content was calculated using the soil mass roughly forty-five minutes after completing the storm event.

The dry bulk density of each soil was calculated before each storm event. The dry soil mass was divided by the volume of soil before starting the storm event to achieve this value. The initial gravimetric moisture content was then multiplied by the dry bulk density and divided by the density of water at the average lab temperature to find the initial volumetric water content. The final gravimetric moisture content was multiplied by the dry bulk density and divided by the density of water at the average lab temperature to find the final volumetric water content.

3.8 X-Ray CT Scanning

One column with biochar and one column without biochar were selected to X-ray scan for the soil types selected. These include CA-2, NC-1, and CA-3. The replicates to be scanned were selected to be closest to the average steady state percolation rate for the three biochar and three control columns. These columns underwent a storm event, where the same procedure described in section 3.3 was followed. The base plate of each column was grinded down before the storm event to ensure the sealed column fit in the X-Ray scanner. The mass and volume of each column were determined before the storm event, immediately after, roughly 45 minutes after completing the storm event, and after X-Ray scanning. The mass of pore water was also determined immediately after and roughly 45 minutes after the storm event. The columns to be scanned were sealed after the measurements were taken, roughly 50 minutes after completing the storm event when most pore water had drained. All holes on the column were covered with electrical tape and packing tape. Parafilm was placed atop the soil surface to protect the soil surface from shifting or leaking. The runoff tube was removed to allow for a cap. A cap was placed atop the column that covered the outlet hole halfway to avoid the cap getting stuck due to suction. The cap was then sealed using electrical tape and packing tape, as noted in Figure 3.4. The Rigaku GX 130 CT Scanner (Rigaku, Tokyo, Japan) was used to scan the columns. The entire column volume was scanned at a resolution of 144 μm. These X-Ray scans can show the soil structure and qualitatively observe soil cracking throughout the entire column.

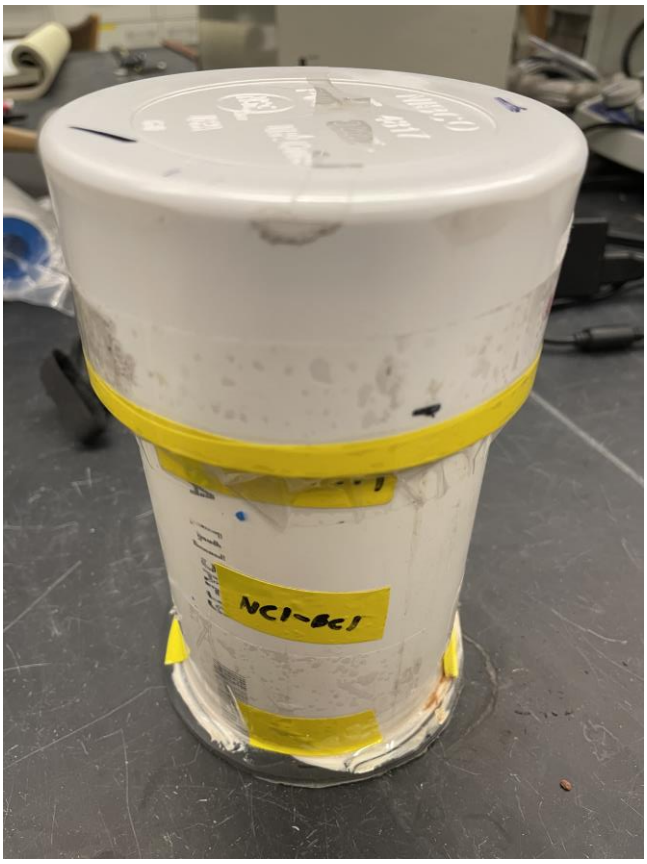

Figure 3.4: NC-1 biochar-amended column sealed and ready to scan.

3.9 Summary of Events

Figure 3.5 showcases the measurements taken and actions performed throughout the experiment duration.

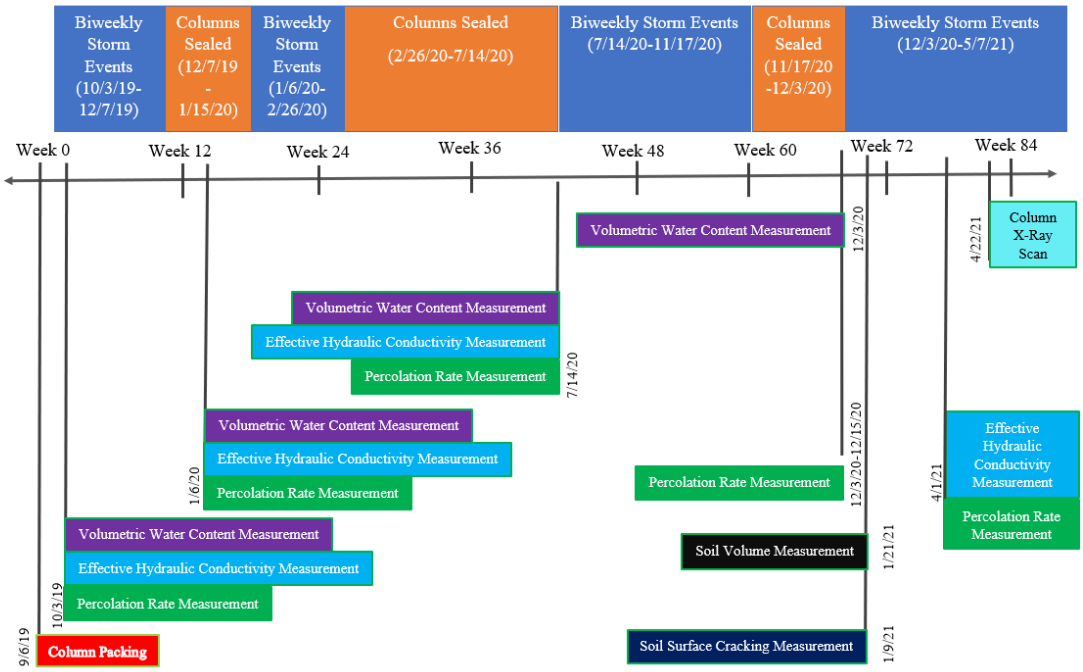

Figure 3.5: Timeline of Actions Performed.

Chapter 4

RESULTS

4.1 Storm Events

4.1.1 Steady-state percolation rate

The total steady state percolation rate divided by total inflow rate versus time after storm one is plotted for each soil type in Appendix A. For DE-1, columns with biochar had higher steady state percolation values than columns without biochar for most of the experiment duration, as seen in Figure A.2. The ratio of steady state percolation rate to inflow rate increased throughout the experiment duration for both control and biochar columns. This increase is most significant from the time Reid stopped these experiments in early 2020 to when he continued them in July 2020. While I have been performing these experiments, the ratio of steady state percolation rate to inflow rate has not increased or decreased sharply. For the DE-2 soil, biochar addition has not had a significant effect on the steady-state percolation rate of any columns. While I have been performing the storm events, biochar-amended soils have had higher steady-state infiltration values for DE-3 soils.

Figure 4.1 shows the average of total steady-state percolation rate of all three replicates divided by the total inflow rate of all three replicates for all soils during for storms 18 through 20. The last three flow measurements were assumed to be steady state conditions for all soil columns since the average percolation rate of three replicates remained at an almost-constant value during that time, as seen in Figure A.1. From these storm events, biochar-amended soils had increased steady-state percolation rate values compared to soils without biochar in six out of 12 soil types.

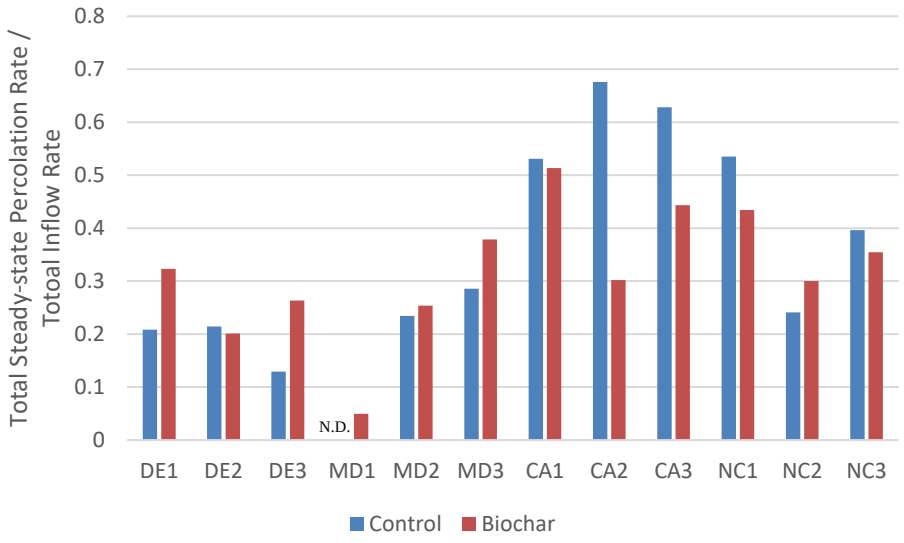

Figure 4.1: Average of total steady-state percolation rate divided by total inflow rate for all soils in storms 18-20.

Biochar addition has had the most visible effect on MD-1 soil. Columns without biochar only experienced percolation for one storm event throughout the experiment duration. Since MD-1 control columns did not experience percolation during storms 18-20, that soil type is labeled N.D. in Figure 4.1. MD-1 columns with biochar have, however, experienced percolation since I began performing storm events. The ratio of steady state percolation rate to inflow rate increased significantly after the columns underwent the first storm event after sealing the columns in early 2020. This ratio has decreased to a constant range since Fall 2020. Biochar addition has not had much of an effect on the steady state percolation rate for MD-2. As seen in Figure 4.2, the ratio of steady state percolation rate to inflow rate has increased due to disruption, then decreased. The ratios for control and biochar-amended columns have increased or decreased to similar values throughout the experiment duration. For MD-

3 soils, biochar-amended soils experienced higher ratios of steady state percolation rate to inflow rate for storm events in the second half of 2020. However, the two most recent storm events have contained a higher ratio for control columns compared to biochar-amended columns.

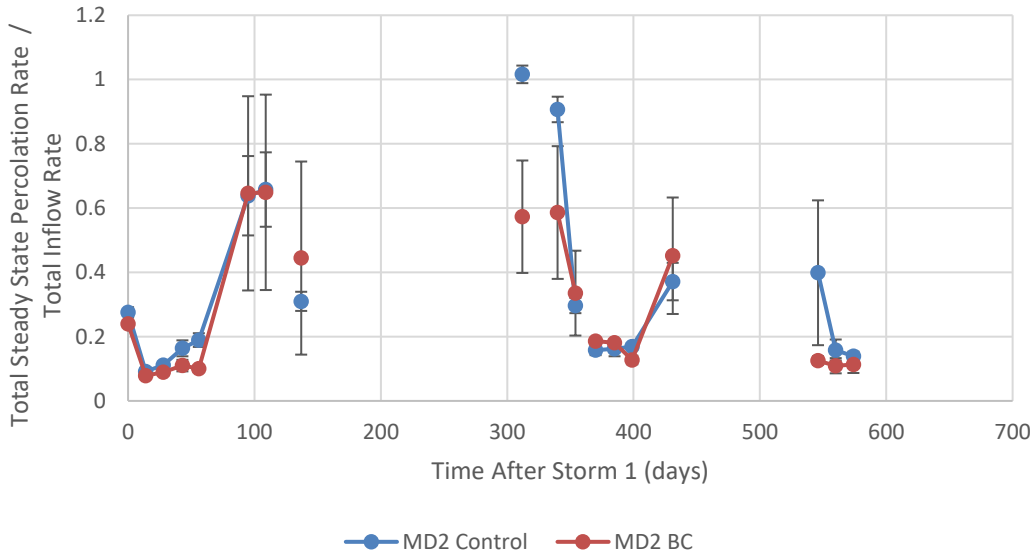

Figure 4.2: Steady State percolation rate for MD-2 with error bars representing the standard error from 3 replicates.

Further, for the CA-1 soil, columns without biochar had a higher ratio of steady state percolation rate to inflow rate during the first nine storm events, as noted by the higher values for control soils from days zero to 137 in Figure 4.3. However, both biochar-amended and columns without biochar have had very similar ratios from September 2020 to the most recent storm event on April 22, 2021, as seen from days 370 to 559 in Figure 4.3. For CA-2, columns without biochar have had a higher ratio of steady state percolation rate to inflow rate for the entire experiment duration. The

same can be said for CA-3 and NC-1 columns. The biochar-amended columns for NC-2 have had a higher ratio of steady state percolation rate to inflow rate compared to columns without biochar for storm events beginning in July 2020. This ratio has also increased significantly since the beginning of the experiment and increased up to the last storm event in 2020. For the two most recent storm events, this ratio has remained nearly the same for biochar-amended columns and has slightly decreased for columns without biochar. For NC-3, storm events taking place before the COVID shutdown consistently showed biochar-amended soils having higher ratios of steady state percolation rate to inflow rate, as seen in Figure 4.4. However, the ratio for biochar-amended soils has increased, and most recent storm events show biochar-amended soils having a higher ratio.

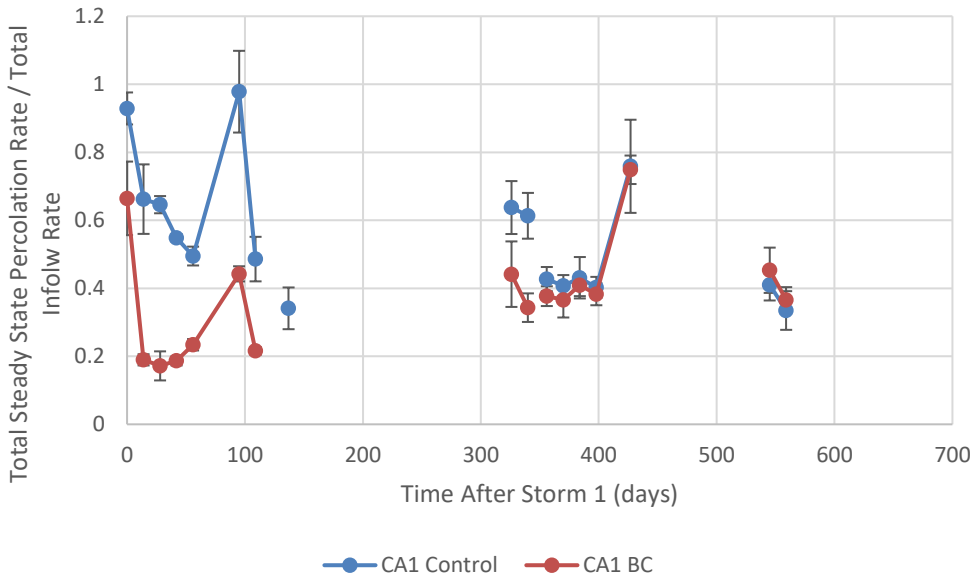

Figure 4.3: Steady state percolation rate for CA-1 with error bars representing the standard error from three replicates.

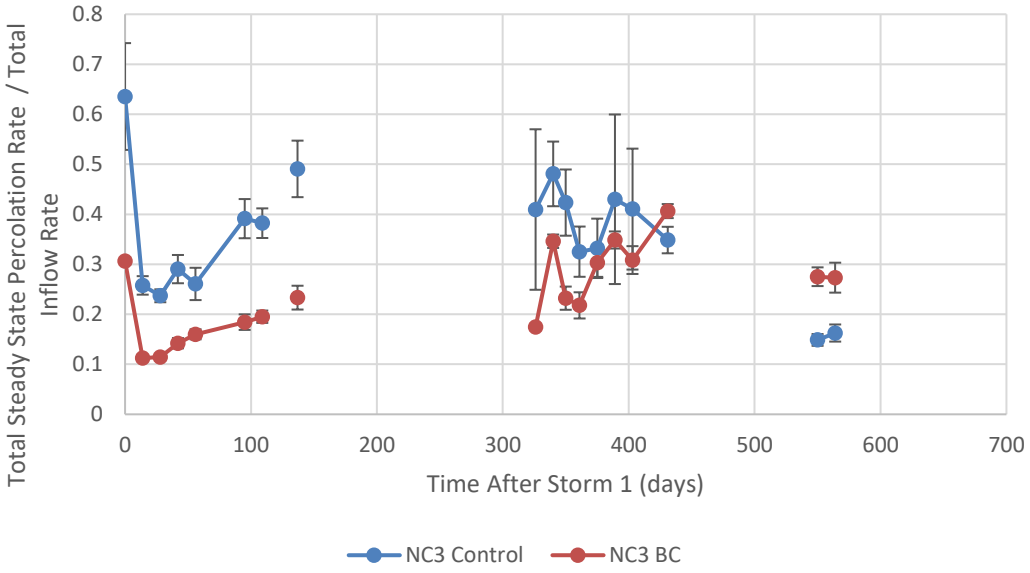

Figure 4.4: Steady state percolation rate for NC-3 with error bars representing the standard error from three replicates.

Steady state percolation rate is important, but further parameters must be investigated to determine whether the addition of biochar to soil can improve soil properties.

4.1.2 Soil Volume

The volume of soil in each column was measured before each storm event starting with storm 22. The volume of soil immediately after each storm event and roughly 45 minutes after each storm event was measured for storms 22 through 27. The volume of nearly all columns increased immediately after the storm compared to the initial volume, then decreased after roughly 45 minutes. Figures 4.5 through 4.7 show the average percent change of soil volume before and immediately after storms

22 through 24 for all soils, respectively. Columns without biochar experienced a higher percentage of soil volume increase for nearly all soils. CA-2 columns without biochar experienced the most significant volume change, at over 4% during storm 24. NC-3 columns without biochar also experienced consistently high volume change at over 2%. MD-1 columns with biochar experienced higher volume change immediately after the storm event than columns without biochar during storm 23. However, MD-1 columns without biochar experienced higher volume change during storms 22 and 24.

Most biochar-amended columns experience volume change less than 2%. Of the columns with biochar, CA-2 experiences the most significant volume change. NC-3, NC-1, and MD-2 columns without biochar show the least percent volume change immediately after each storm event compared to before that storm event.

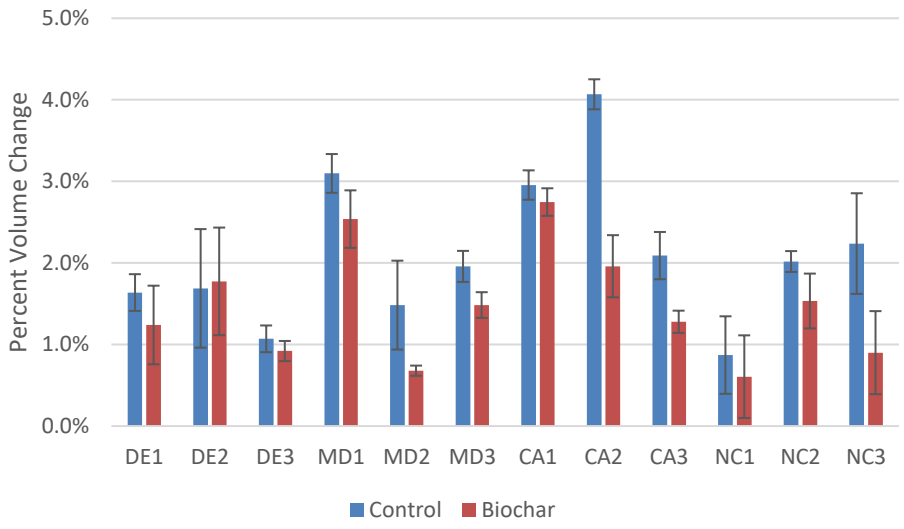

Figure 4.5: Percent volume change before and immediately after storm event for storm 22 with error bars representing the standard error from three replicates.

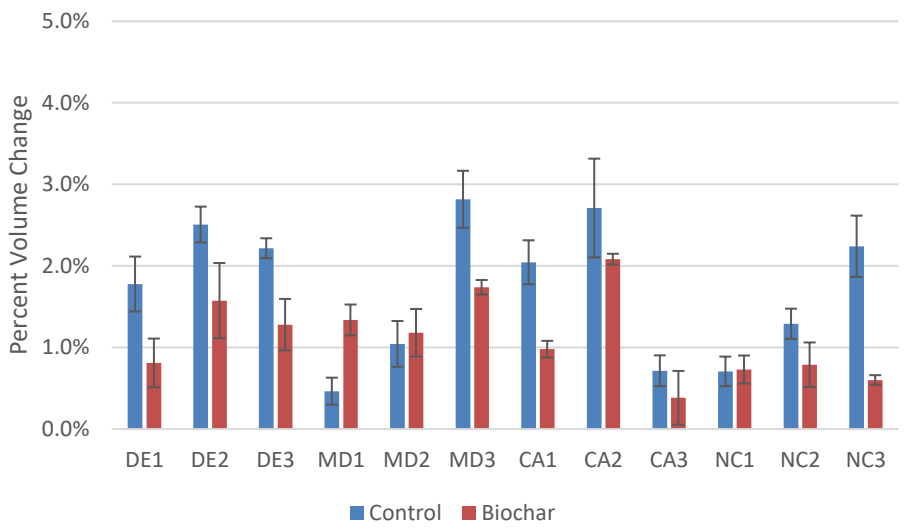

Figure 4.6: Percent volume change before and immediately after storm event for storm 23 with error bars representing the standard error from three replicates.

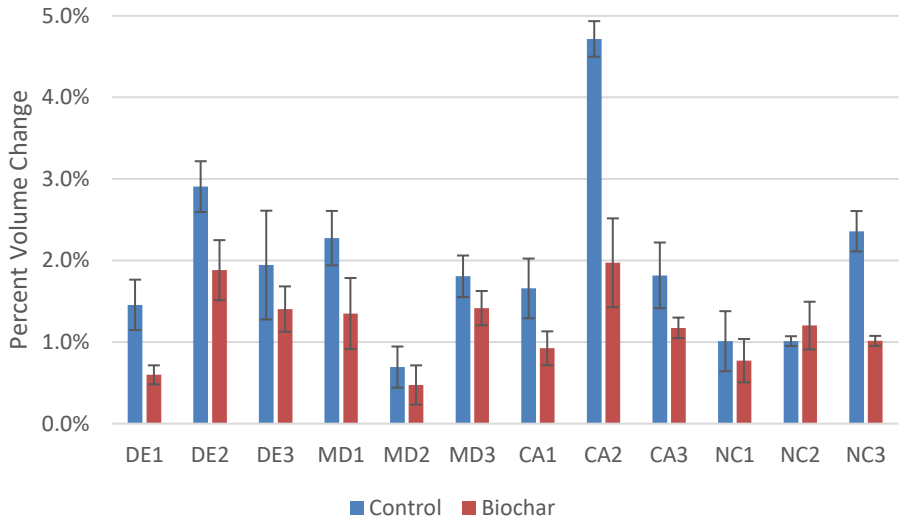

Figure 4.7: Percent volume change before and immediately after each storm event for storm 24 with error bars representing the standard error from three replicates.

4.1.3 Soil Surface Cracking

The surface of nearly every column featured cracks before each storm event. These cracks were filled in immediately after the storm event for almost all columns. Three total replicates of CA-2 and CA-3 columns without biochar experienced surface cracking after the storm event. Figures 4.8 through 4.10 show the percentage of the column surface with cracks before storms 22, 23, and 24 for each soil type, respectively. CA-2 soils without biochar consistently had the highest area of cracks, at over 8% for storms 23 and 24. Replicates with biochar consistently showed more cracking than replicates of the same soil type without biochar. Of the biochar-amended soils, CA-2 had the most cracking, at up to 3.73% of its surface area before storm 23. DE-1, MD-2, CA-3, and NC-1 biochar-amended soils consistently showed less than 2% of surface area featuring cracks before storms 22 through 24. Of the soils without biochar, DE-1, MD-2, and NC-1 consistently showed less than 2% of surface area featuring cracking before storms 22 through 24.

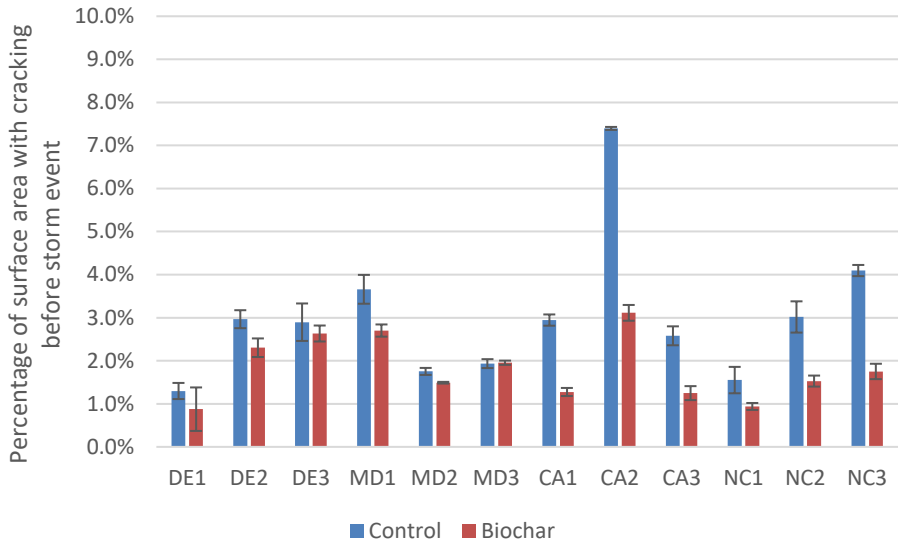

Figure 4.8: Percentage of soil surface with cracks before storm 22 with error bars representing the standard error from three replicates.

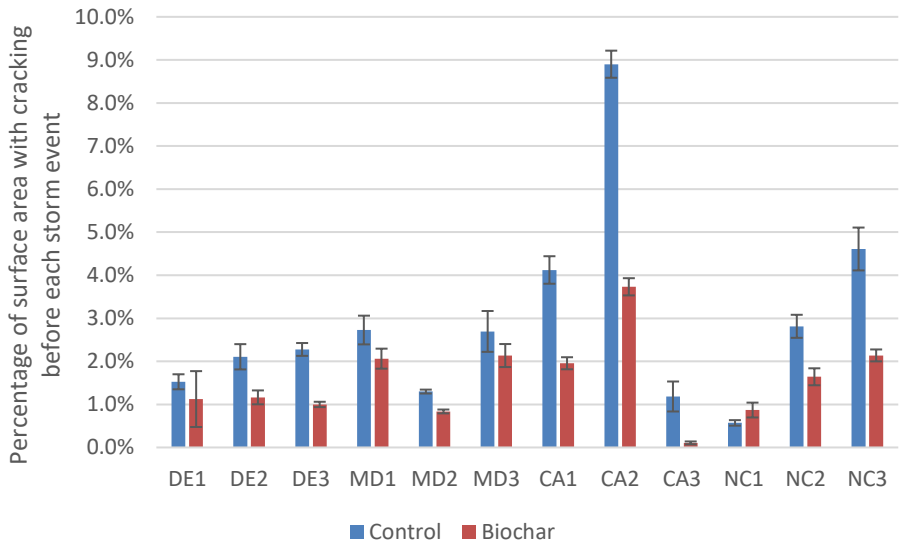

Figure 4.9: Percentage of soil surface with cracks before storm 23 with error bars representing the standard error from three replicates.

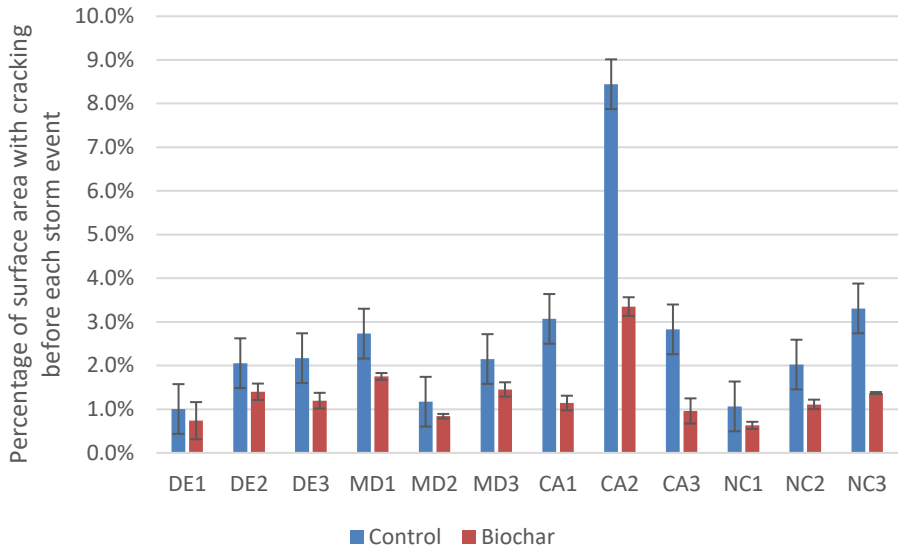

Figure 4.10: Percentage of soil surface with cracks before storm 24 with error bars representing the standard error from three replicates.

4.1.4 Volumetric Water Content

The volumetric water content was measured before each storm event and roughly 45 minutes after each storm event after most pore water had drained out. The volumetric water content decreased during this period. Figures B.1 through B.10 show the average change in volumetric water content versus time for each soil. The percent change in volumetric water content for biochar-amended soils was higher than that for soils without biochar for all soils. The percent change in volumetric water content for both control and biochar-amended soils also decreased over time. The average change in volumetric water content was often very similar at each individual storm event between control and biochar-amended columns. Figure 4.11 shows the average change in volumetric water content versus experiment duration for CA-2 replicates, which are similar for control and biochar-amended replicates at each measurement date. MD-3, MD-1, and DE-1 are the soils the greatest difference between change in volumetric

water content between control and biochar-amended columns at an individual storm event. Figure 4.12 shows the average change in volumetric water content versus experiment duration for MD-1 replicates. MD-1 columns without biochar did not experience any percolation throughout most of the experiment duration, so the change in volumetric water content is expected.

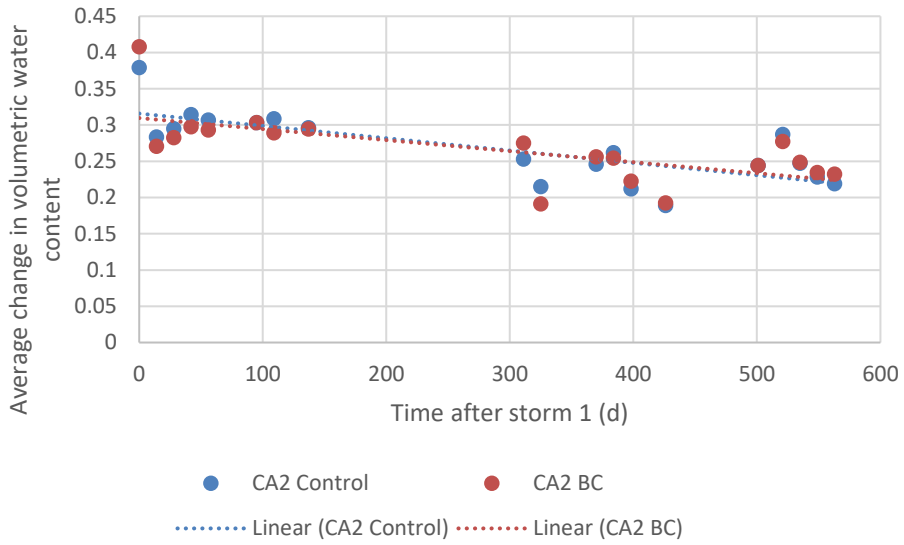

Figure 4.11: Average change in volumetric water content versus time for CA-2.

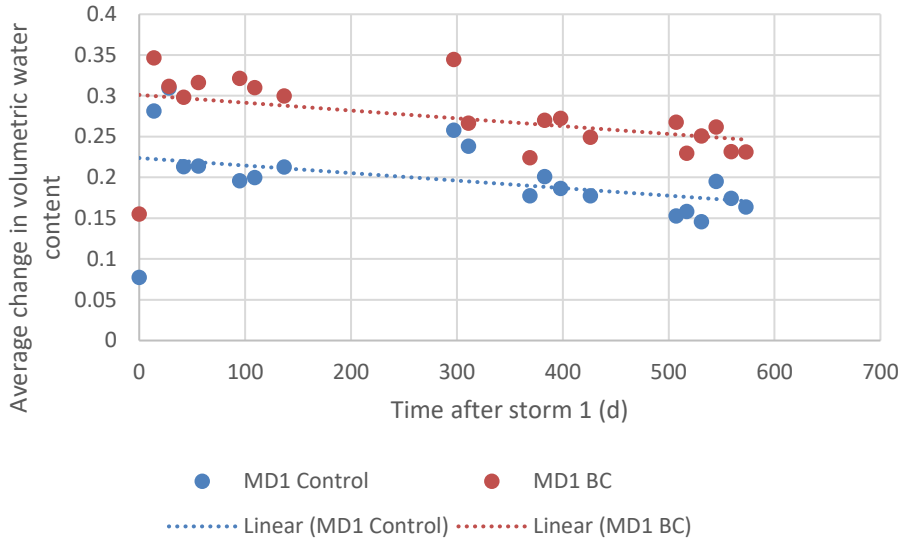

Figure 4.12: Average change in volumetric water content versus time for MD-1.

Chapter 5

DISCUSSION

5.1 Biochar/Control Effective Hydraulic Conductivity Ratio

The effective hydraulic conductivity, K_{sat} was calculated for each storm event when runoff was also recorded. The following equation was used.

$$K_{sat} = \frac{Q\Delta L}{A\Delta H} \quad (5\text{-}1)$$

Q is equal to the steady state percolation rate, A is the cross-sectional area of the column, ΔL is the soil height, and ΔH is the distance between the ponded water level and the bottom of the soil, which is where water drips out into the bottom chamber of the column before dripping out through the effluent hole. The ratio of effective conductivity hydraulic for biochar-amended soils to control soils was compared with the volume change of control soils. Figures 5.1 through 5.3 show the relation between volume change in control soils and the ratio of biochar to control effective hydraulic conductivity (BC/C K_{sat} ratio). The BC/C K_{sat} ratio was the average from storms 18 to 20 since steady state percolation rate was not measured from storms 21 through 25. Figures 5.1 through 5.3 show data for 11 out of 12 soils. MD-1 was excluded since the MD-1 soils without biochar did not have any percolation.

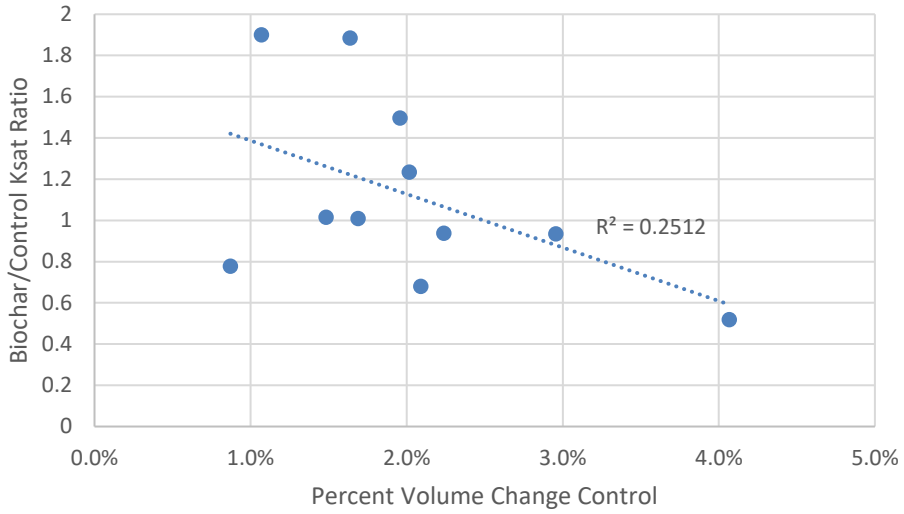

Figure 5.1: Biochar/control K_{sat} ratio versus percent volume change of control soils for storm 22.

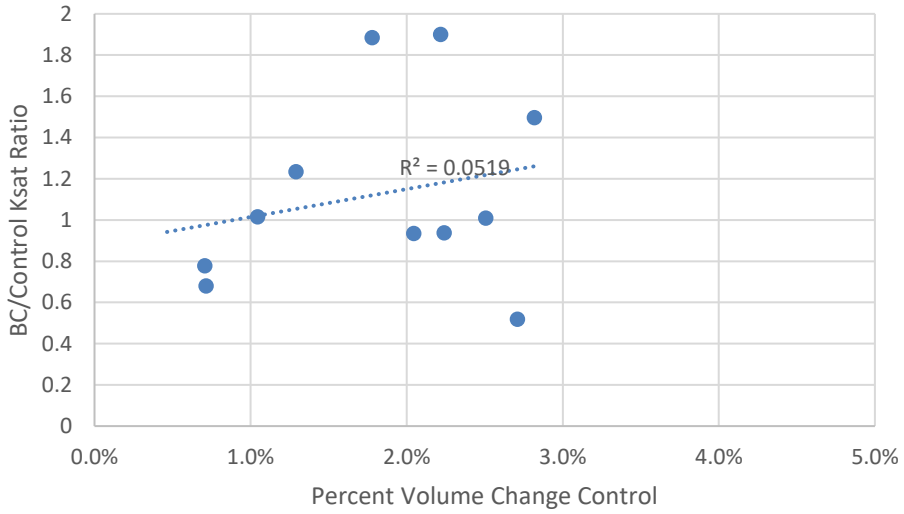

Figure 5.2: Biochar/control K_{sat} ratio versus percent volume change of control soils for storm 23.

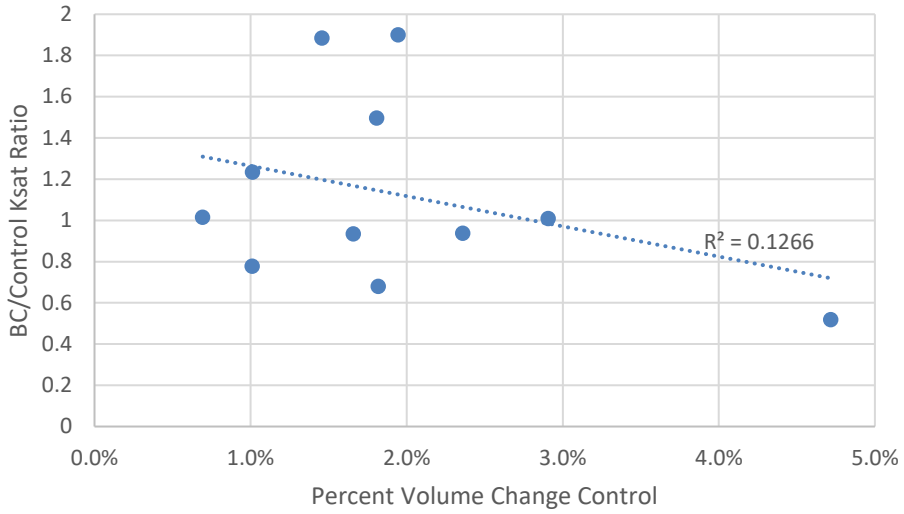

Figure 5.3: Biochar/control K_{sat} ratio versus percent volume change of control soils for storm 24.

There is a slight negative correlation between BC/C K_{sat} ratio and percent volume change in control soils in storms 22 and 24. This means that if K_{sat} values are higher for biochar-amended replicates compared to control replicates for one soil type, control soils will have less volume change. Similarly, if K_{sat} values are higher for control replicates compared to biochar-amended replicates for one soil type, control soils will have greater volume change. This shows that the effective hydraulic conductivity of control soils and the volume change of control soils are proportional.

5.2 Gravimetric Moisture Content Relations

A relation between gravimetric moisture content and soil surface cracking was observed. Soils with lower gravimetric moisture contents were expected to have a higher percentage of soil surface cracks than soils with higher gravimetric moisture

contents. The percentage of cracking surface area versus initial moisture content for all soils was plotted for storms 23 through 25, as seen in Figures C.1 through C.10. For Delaware and Maryland soils, most soils with biochar had slightly higher initial moisture contents and slightly lower cracking. There were no large separations in data between control and biochar columns, as seen in Figure 5.4, which shows soil cracking surface area versus initial moisture content for DE-2 in storms 23 through 25. For CA-1, CA-2, NC-2, and NC-3, there were stark differences in control and biochar columns. Columns with biochar had significantly higher moisture content and significantly lower cracking for these soils. Figure 5.5 shows this relation for CA-2, with biochar-amended replicates having consistently higher change in moisture content and significantly lower soil surface cracking.

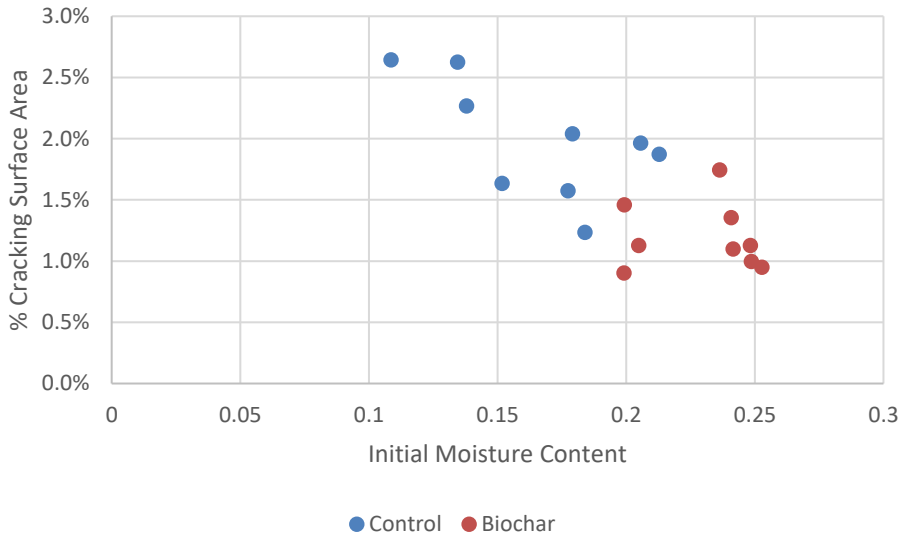

Figure 5.4: Soil cracking surface area versus initial gravimetric moisture content for DE-2 in storms 23 through 25.

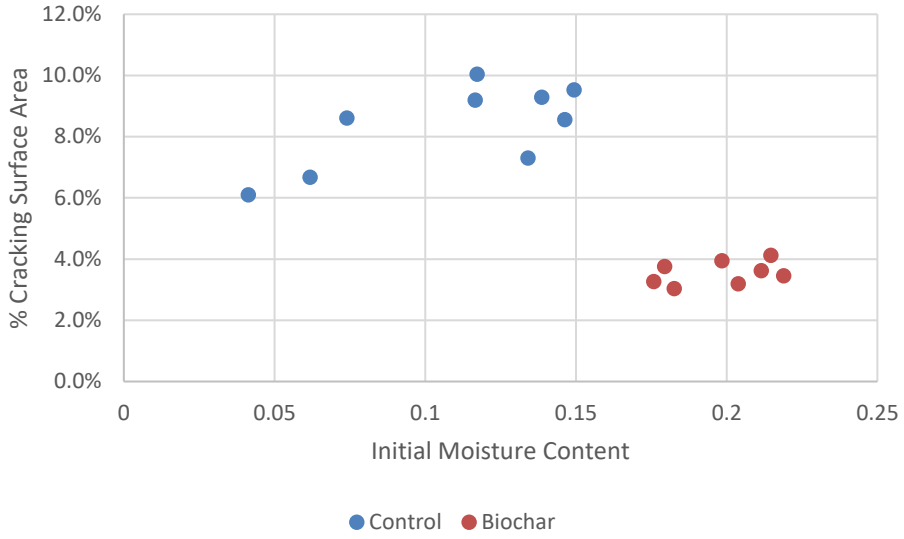

Figure 5.5: Soil cracking surface area versus initial gravimetric moisture content for CA-2 in storms 23 through 25.

The relation between gravimetric moisture content and soil volume was also observed. Soil volume change from before the storm event to immediately after the storm event was plotted versus the change in moisture content from the before the storm event to roughly 45 minutes after the storm event finished. Figures C.11 through C.20 show these plots with data from storms 23 through 25. Columns with biochar had significantly higher changes in moisture content compered to columns without biochar but had lower volume change. DE-1 replicates showed biochar-amended soils with higher change in gravimetric moisture content for all biochar-amended replicates except for one, and typically lower volume change, as seen in Figure 5.6. MD-1 control soils had significantly lower changes in moisture content compared to biochar-amended soils, but had roughly the same distribution of volume change, as seen in Figure 5.7.

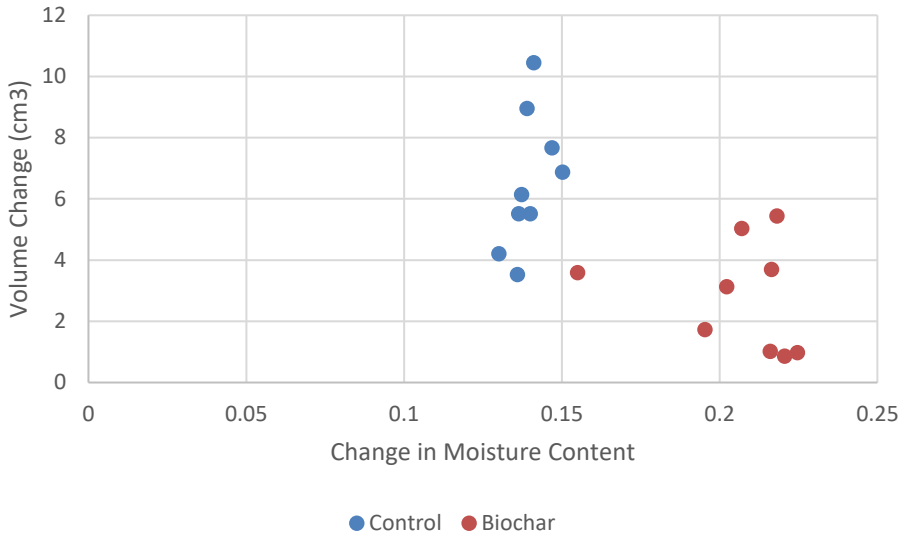

Figure 5.6: Volume change in gravimetric moisture content for DE-1 in storms 23 through 25.

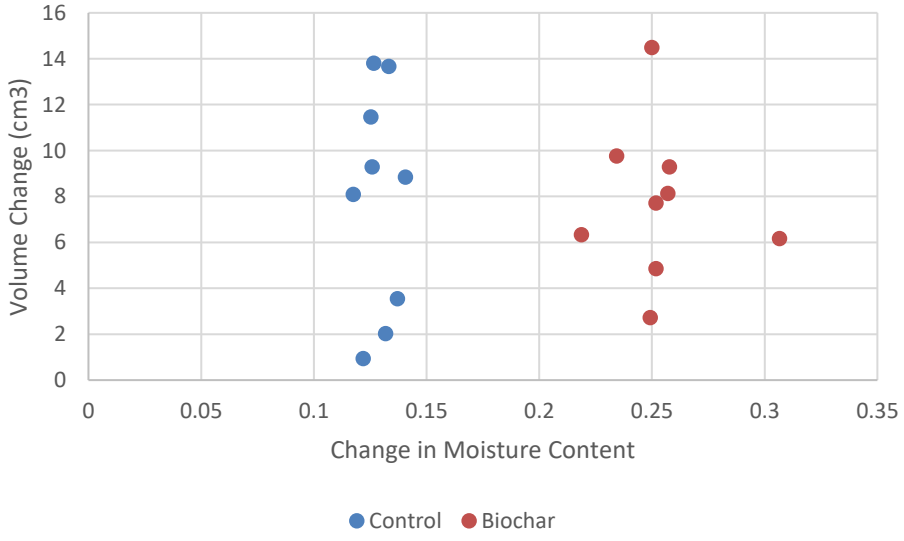

Figure 5.7: Volume change versus change in gravimetric moisture content for MD-1 in storms 23 through 25.

5.3 Soil Cracking and X-Ray Analysis

NC-1, CA-2, and CA-3 were selected to be X-Ray scanned due to the application of biochar affecting each of these soils differently. Biochar-amendment decreased the steady state percolation rate of NC-1, while both control and biochar-amended soils experienced low surface cracking. For CA-2 columns, biochar-amendment slightly decreased the steady state percolation rate, while control soils experienced very high cracking. CA-2 biochar-amended soils also experienced the highest percentage of soil surface cracking compared to the other biochar-amended soils. Biochar amendment did not have much of an effect on the steady state percolation rate on CA-3 columns. CA-3 control and biochar-amended soils also experienced near-average soil surface cracking compared to the other control and biochar-amended soils.

Figure 5.8 shows X-Ray images of NC-1 columns. The bottom left and right images in this figure show roughly 30% of the circular soil area at roughly 4.3 cm below the soil surface for an NC-1 replicate without biochar and a biochar-amended replicate, respectively. The 6 mm-thick column walls can be seen on the right side of both X-Ray images. High-density materials such as soil particles appear as white in the X-Ray images. Air-filled spaces appear as black, while ranging shades of gray could be water-filled biochar particles or low-density soil particles. There are small cracks present in the NC-1 replicate without biochar, as seen by the small black voids near the column wall and the black voids toward the center of the bottom-left image in Figure 5.8. In the bottom-right image of Figure 5.8 representing the biochar-amended NC-1 replicate, there are dark gray areas, but no black voids representing cracks. Figure 5.9 shows the same relation for CA-3 replicates. The bottom-right image in Figure 5.9, representing the CA-3 replicate without biochar, also shows air-filled

spaces around the column wall. The biochar-amended CA-3 replicate shows gray areas which are not classified as cracks. This suggests that biochar application does not only reduce the amount of soil cracking at the surface; it reduces cracking throughout the soil volume.

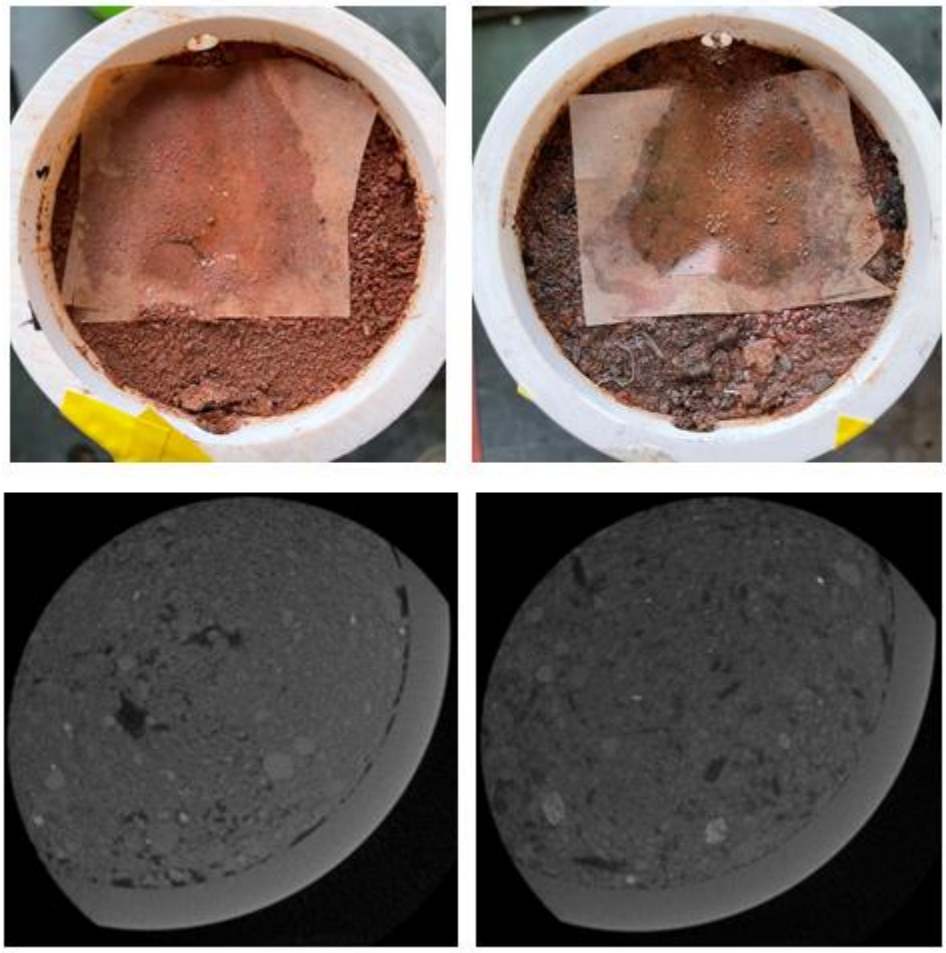

Figure 5.8: Top left: NC1-1 surface immediately after storm event, Bottom left: NC1-1 X-Ray scan roughly 4.3 cm from soil surface, Top right: NC1-BC1 soil surface, Bottom right: NC1-BC1 X-Ray scan roughly 4.3 cm from soil surface.

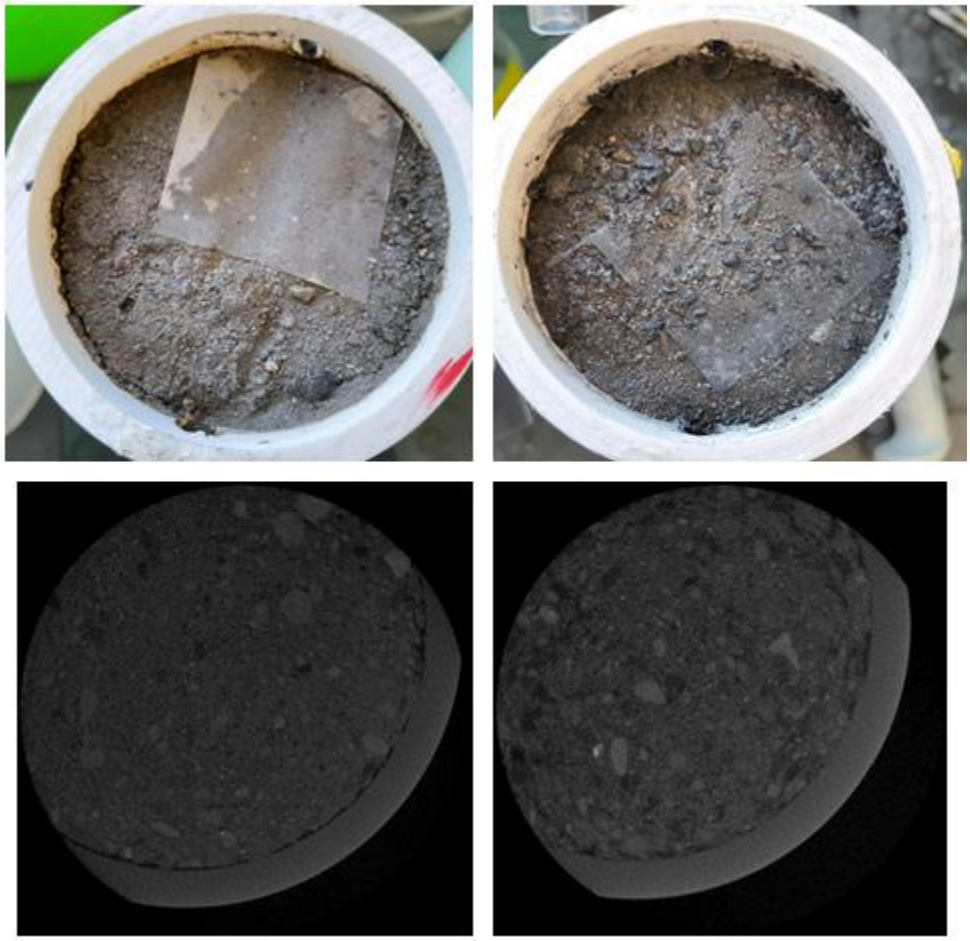

Figure 5.9: Top left: CA3-2 surface immediately after storm event, Bottom left: CA3-2 X-Ray scan roughly 4.3 cm from soil surface, Top right: CA3-BC3 surface immediately after storm event, Bottom right: CA3-BC3 X-Ray scan roughly 4.3 cm from soil surface.

Figures 5.10 and 5.11 show the X-Ray images taken from NC-1 and CA-3 replicates roughly 1 cm from the column surface, respectively. Both images show roughly 30% of the circular soil area. There are air-filled spaces around the column wall in the NC-1 replicate without biochar, as shown in the left image in Figure 5.10. There are also small pores toward the center of the columns shown by the black

circular voids toward the top left of this image. For the NC-1 replicate without biochar, there are very small black voids representing cracks next to the column wall. Since there are more visible cracks in the control replicate at a depth of nearly 1 cm along with the cracks shown in Figure 5.8, this further supports the notion that biochar-amendment reduces cracks throughout the soil volume. The X-Ray scans for CA-3 replicates are shown in Figure 5.11, where the biochar-amended replicate has no cracks compared to the control soil.

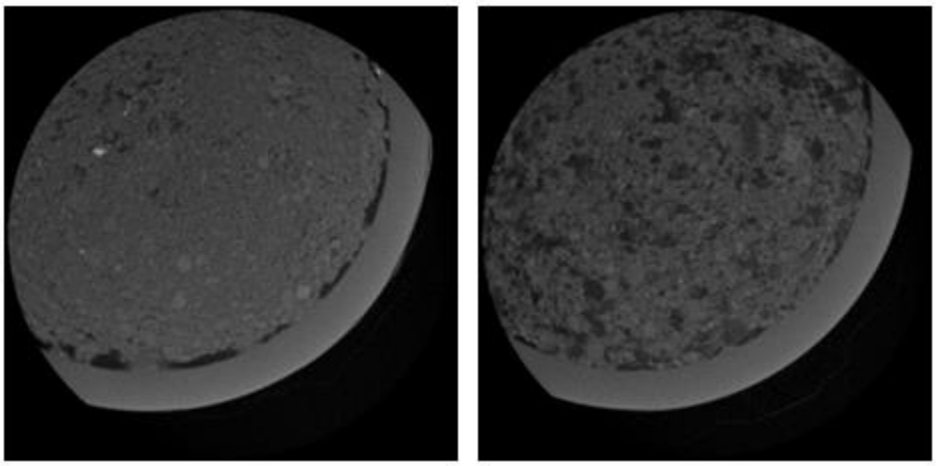

Figure 5.10: Left: NC1-1 X-Ray scan roughly 1 cm from soil surface, Right: NC1-BC1 X-Ray scan roughly 1 cm from soil surface.

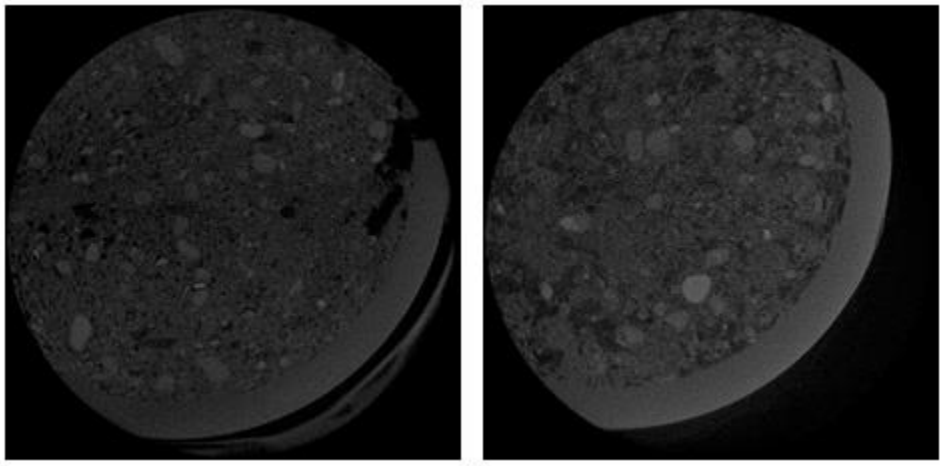

Figure 5.11: Left: CA3-2 X-Ray scan roughly 1 cm from soil surface, Right: CA3-BC3 X-Ray scan roughly 1 cm from soil surface.

Additional scans are currently being performed for additional soil types. Figures 5.12 and 5.13 show the X-Ray images of DE-1 at roughly 4.3 cm from the surface and roughly 1 cm from the soil surface, respectively. The bottom left image in Figure 5.12 shows the X-Ray scan of the DE-1 control replicate roughly 4.3 cm from the soil surface. There are two cracks in this image toward the center of the column, but these cracks are not present in the left image of Figure 5.13, which shows an X-Ray scan of the same replicate roughly 1 cm from the soil surface. This suggests that these are minor cracks that do not have a significant effect on the percolation rate of this replicate. The bottom right image in Figure 5.12 and the right image in Figure 5.13 show an X-Ray scan of a DE-1 replicate with biochar roughly 4.3 cm from the soil surface and roughly 1 cm from the soil surface, respectively. The DE-1 biochar-amended column does not have any cracks at either soil depth. Figures 5.14 and 5.15 show the X-Ray images of DE-3 at roughly 4.3 from the surface and roughly 1 cm from the soil surface, respectively. Small cracks along the column wall are seen for the

DE-3 control replicate roughly 1 cm from the soil surface, represented by the small black voids along the column wall in the left image in Figure 5.15. The biochar-amended DE-3 column also has very minimal cracks along the column wall at roughly 4.3 cm of depth and roughly 1 cm of depth, noted by the small black voids along the column wall in the bottom right image of Figure 5.14 and the right image in Figure 5.15, respectively.

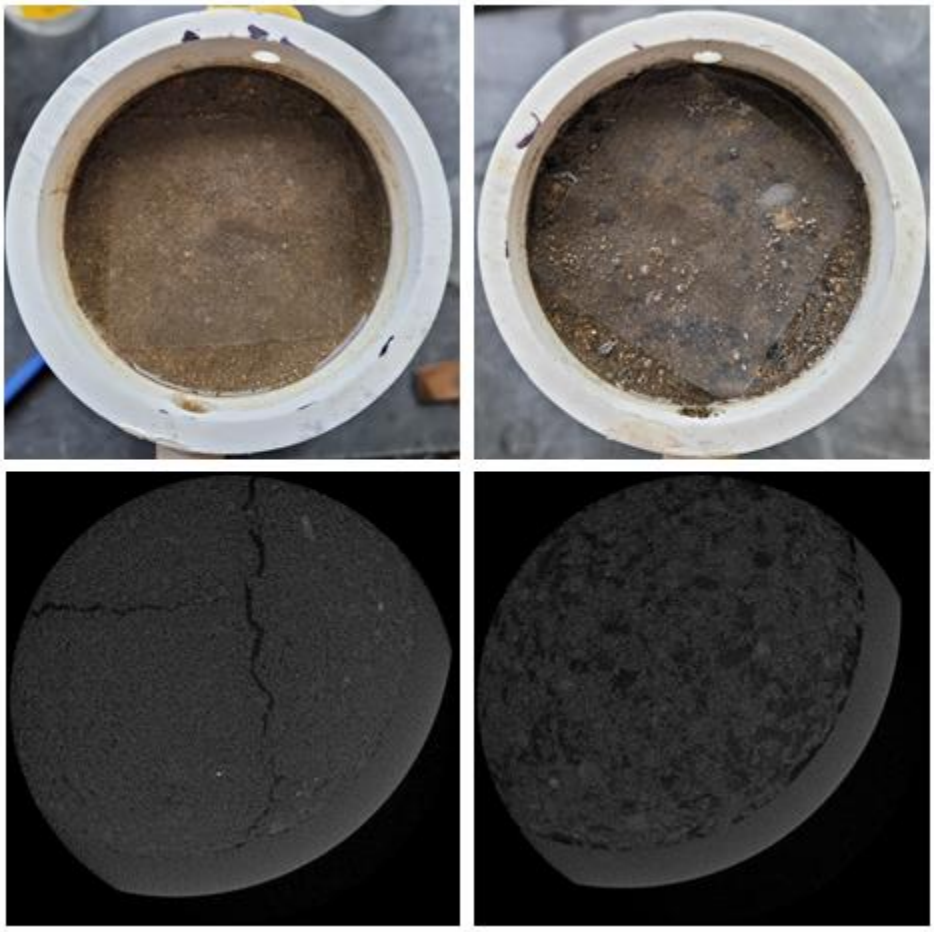

Figure 5.12: Top Left: DE1-3 surface immediately after storm event, Bottom left: DE1-3 X-Ray scan roughly 4.3 cm from soil surface, Top right: DE1-BC3 surface immediately after storm event, Bottom right: DE1-BC3 X-Ray scan roughly 4.3 cm from soil surface.

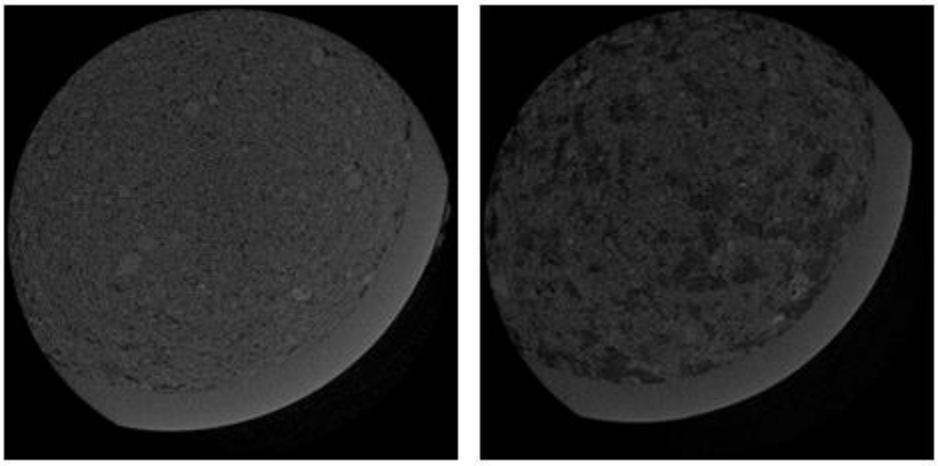

Figure 5.13: Left: DE1-3 X-Ray scan roughly 1 cm from soil surface, Right: DE1-BC3 X-Ray scan roughly 1 cm from soil surface.

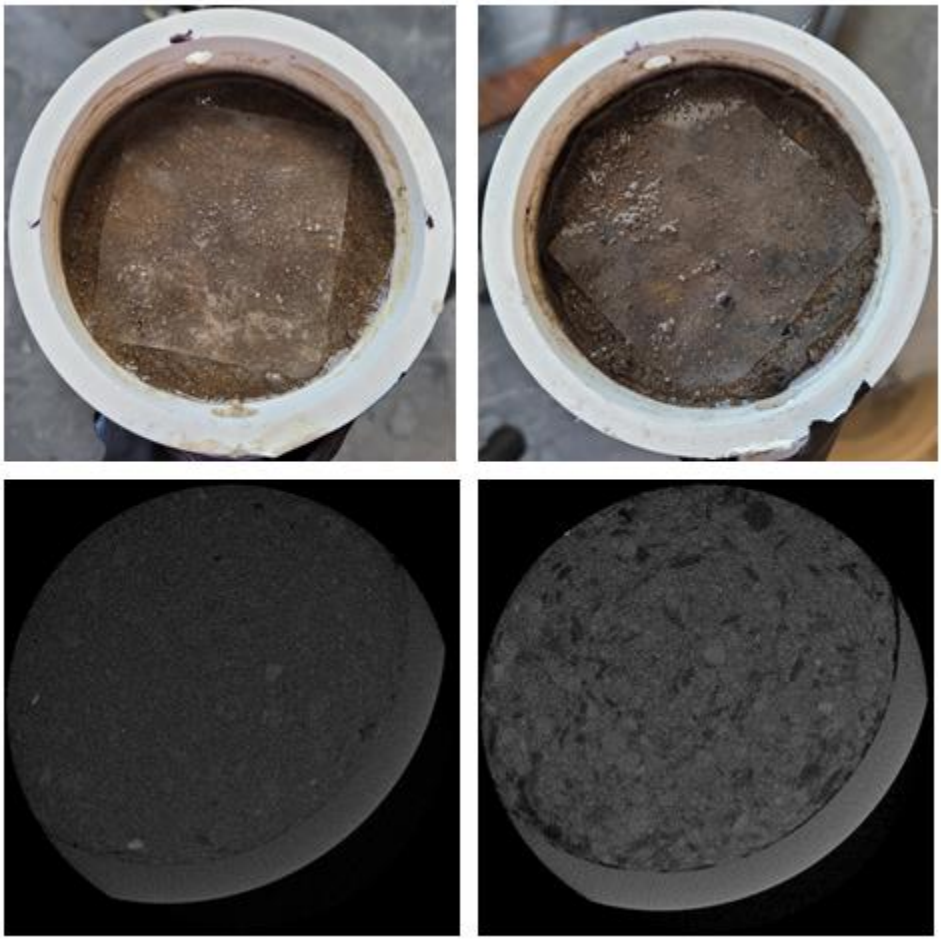

Figure 5.14: Top left: DE3-3 surface immediately after storm even, Bottom left: DE3-3 X-Ray scan roughly 4.3 cm from soil surface, Top right: DE3-BC3 surface immediately after storm event, Bottom right: DE3-BC3 X-Ray scan roughly 4.3 cm from soil surface.

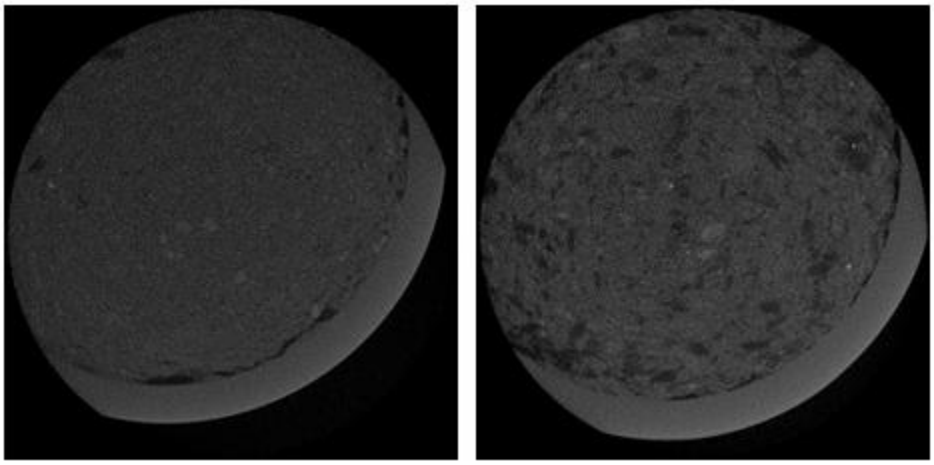

Figure 5.15: Left: DE3-3 X-Ray scan roughly 1 cm from soil surface, Right: DE3-BC3 X-Ray scan roughly 1 cm from soil surface.

Chapter 6

CONCLUSIONS

12 soils from four states were used to test the hypothesis that biochar-amendment would increase the effective hydraulic conductivity through time for some soils due to enhanced soil aggregation. In doing so, the impact of biochar on soil cracking and soil swelling was quantified by images of the soil surface for each replicate and qualitatively viewed by X-Ray scans. Of the NC-1, CA-3, and CA-2 columns scanned, along with additional X-Ray scans of DE-1 and CA-1 replicates, all five replicates without biochar experienced cracking and some biochar-amended replicates had minimal consequential cracking.

The impact of biochar amendment on steady state percolation rate from routine storm events was also quantified. For roughly six out of 12 soils, biochar-amendment has increased steady state percolation rate. These six soils experienced a roughly 30% increase in K_{sat} for biochar-amended soils compared to control soils. If replicates with artificially large percolation rates due to cracking are discarded, biochar-amended soils still have lower steady state percolation rates compared to control replicates, in CA-2 for example. Biochar-amendment has also decreased the volume change in soils before and immediately after a wetting-drying cycle for all soil types by an average of 56.1% for storms 22, 23, and 24. Further, biochar-amendment has decreased the area of surface cracking for all soils.

Comparisons between saturated hydraulic conductivity, volume change, gravimetric moisture content, and soil surface cracking were made. It can be concluded that biochar-amended soils have higher moisture content, lower volume change, and lower overall soil cracking. Future actions will be performed on the same

soil columns to further investigate the effect of biochar on soil properties. One control and one biochar-amended replicate will be X-Ray scanned for all 12 soils to determine whether biochar amendment has the same effect on soil cracking for a wider range of soil types. Each replicate will then be dismantled, and a wet sieve will be used to observe the effect of biochar amendment on soil aggregation.

REFERENCES

ASTM D422. 2007. “Standard Test Method for Particle-Size Analysis of Soils.” Astm. https://doi.org/West Conshohocken, PA.

Bronick, C., Lal, R. (2005, 1). Soil structure and management: a review. Geoderma, 3-22

Davis, A., Kim, H., Seagren, E. (2003). Engineered Bioretention for Removal of Nitrate from Stormwater Runoff. Water Environment Research, 75, 355-367

Landers, J. (2018). Adding Biochar to Soils beside Highways Could Reduce Runoff, Report Says. American Society of Civil Engineers

Lehmann, J., Joseph, S. (2015). Biochar for environmental management: an introduction. Biochar for environmental management, 33-46

Mukherjee, A., Lal, R. (2013). Biochar Impacts on Soil Physical Properties and Greenhouse Gas Emissions. Agronomy, 313-339

Romkens, M., Prasad, S. (2006). Rain Infiltration into swelling/shrinking/cracking soils. Agricultural Water Management, 196-205

Tang, C., Zhu, C., Leng, T., Shi, B. Cheng, Q., Zeng, H. (2019). Three-dimensional characterization of desiccation cracking behavior of compacted clayey soil using X-ray computed tomography. Engineering Geology, 225, 1-10

Williams, R. (2020). The Effect of Biochar Addition on Soil Aggregation and Stormwater Infiltration. University of Delaware Senior Thesis, 9-19

Zhang, Y., Gu, K., Li, J., Tang, C., Shen, Z., Shi, B. (2020). Effect of biochar on desiccation cracking characteristics of clayey soils. Geoderma, 364, 2020

Appendix A

Steady State Percolation Rate

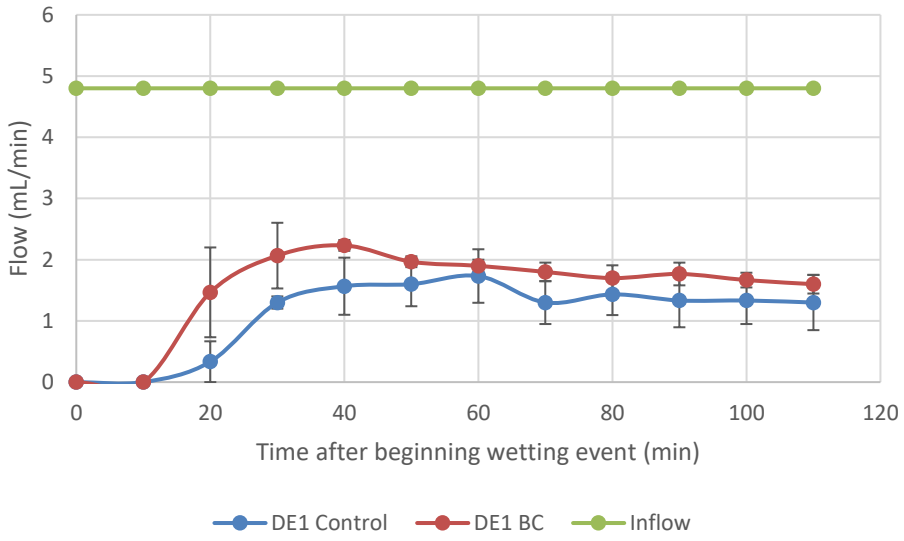

Figure A.1: Average percolation rate for DE-1 Storm 20 with error bars representing the standard error from three replicate values.

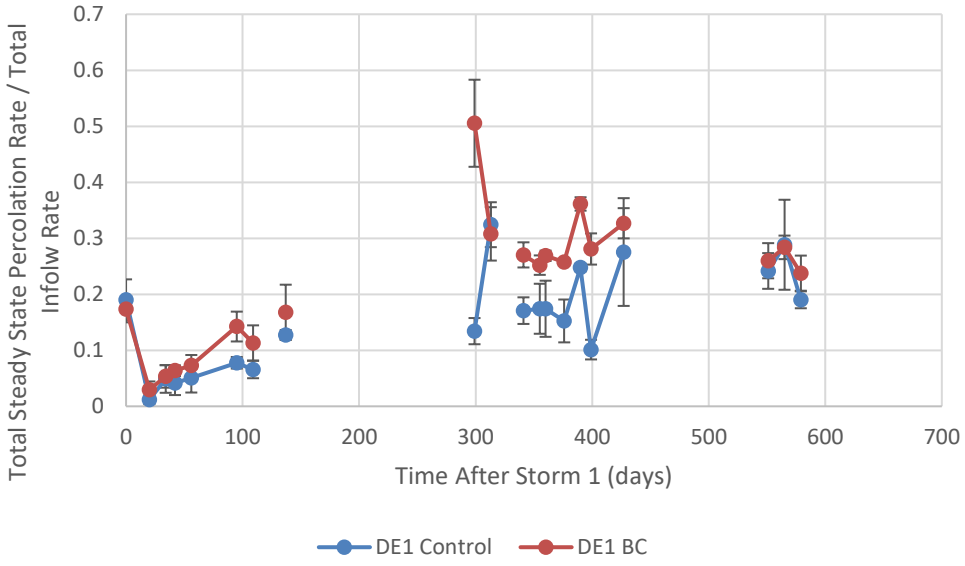

Figure A.2: Steady State percolation rate for DE-1 with error bars representing the standard error from three replicate values.

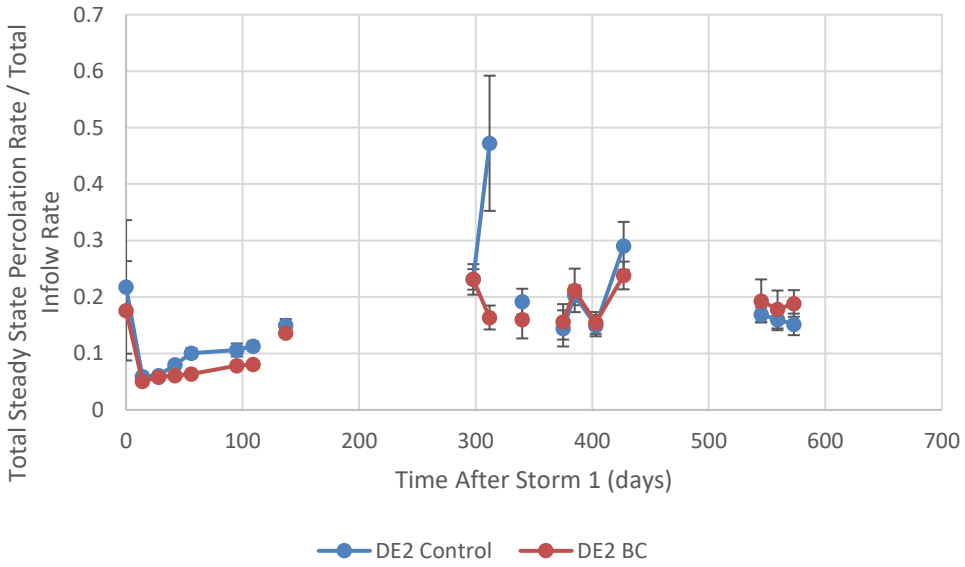

Figure A.3: Steady State percolation rate for DE-2 with error bars representing the standard error from three replicate values.

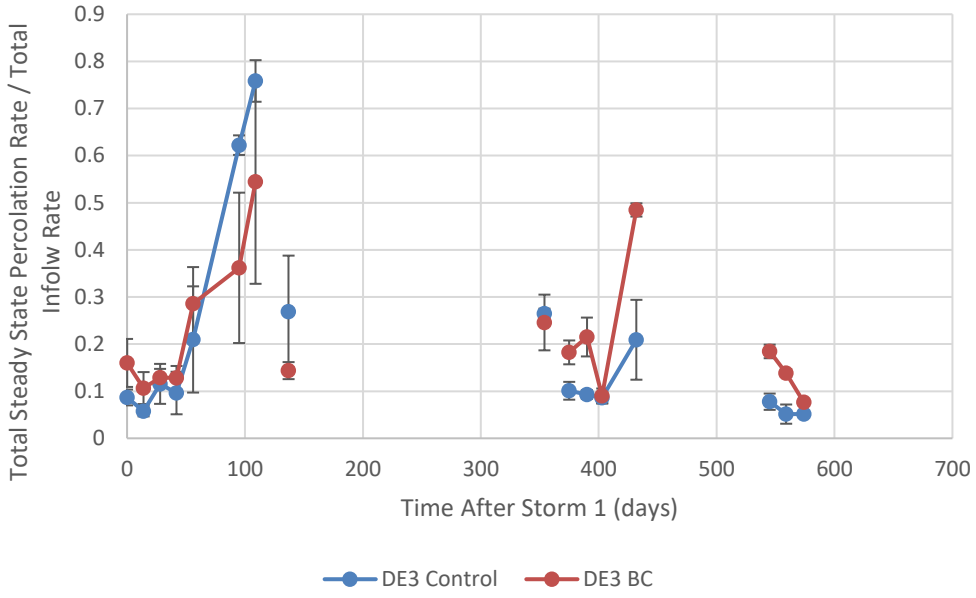

Figure A.4: Steady State percolation rate for DE-3 with error bars representing the standard error from three replicate values.

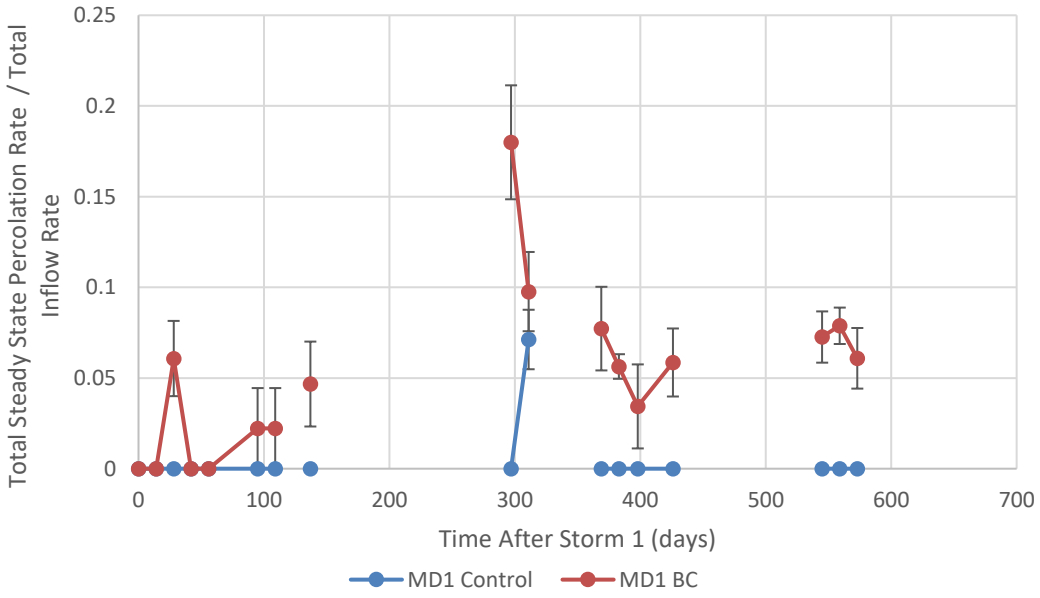

Figure A.5: Steady State percolation rate for MD-1 with error bars representing the standard error from three replicates.

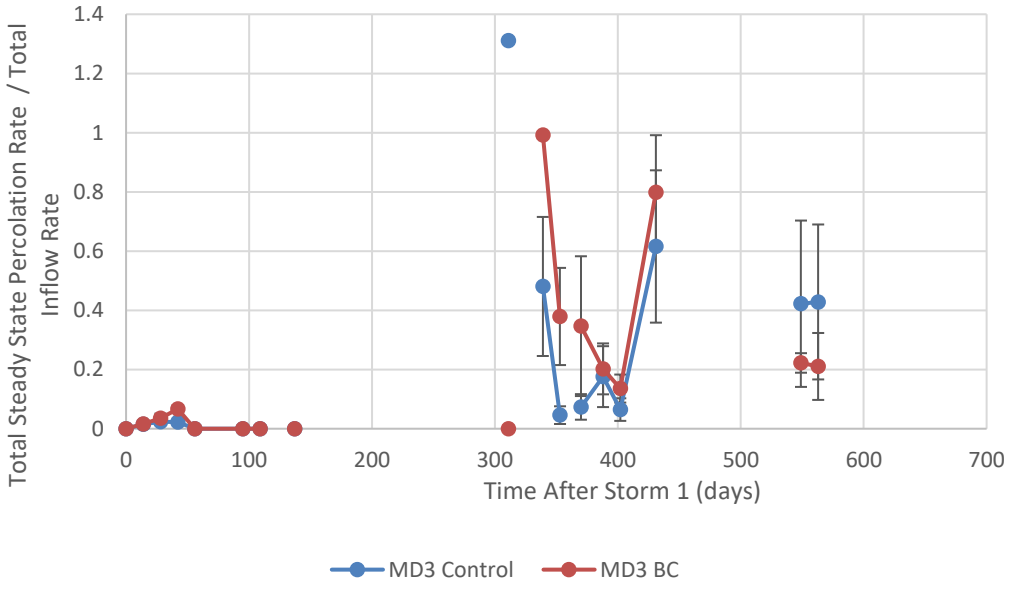

Figure A.6: Steady State percolation rate for MD-3 with error bars representing the standard error from three replicates.

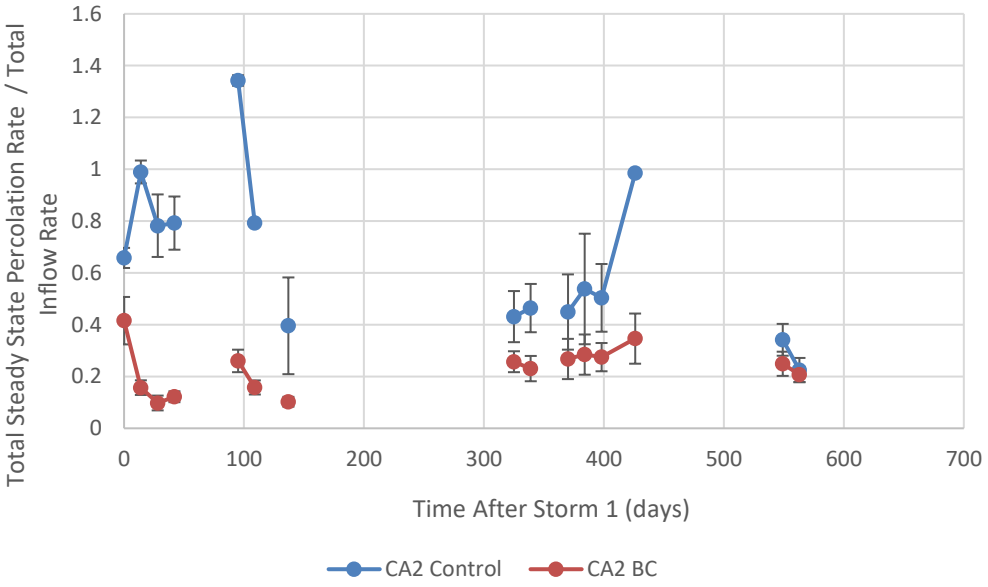

Figure A.7: Steady State percolation rate for CA-2 with error bars representing the standard error from three replicates.

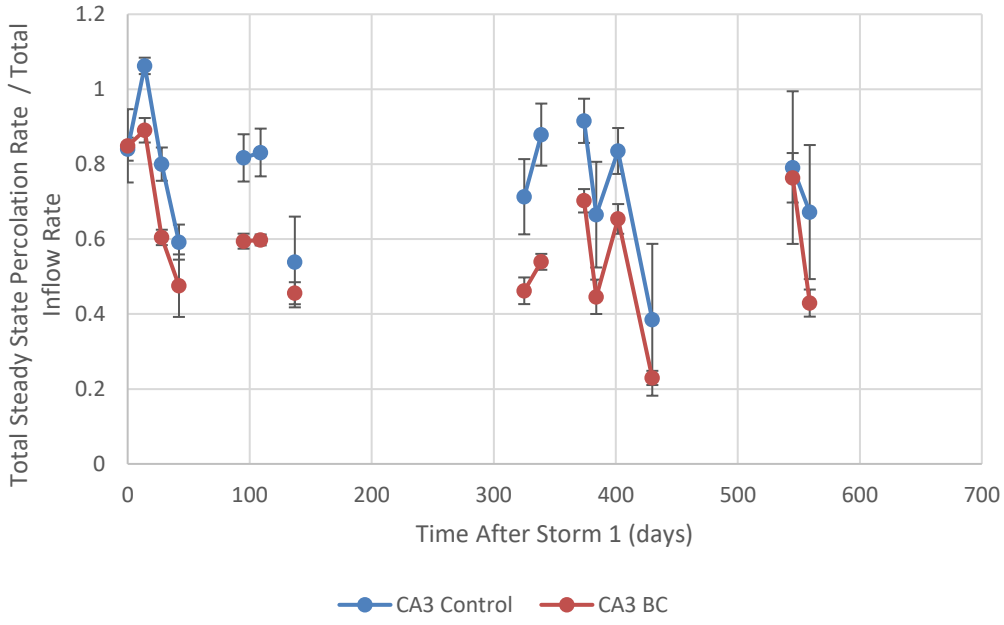

Figure A.8: Steady State percolation rate for CA-3 with error bars representing the standard error from three replicates.

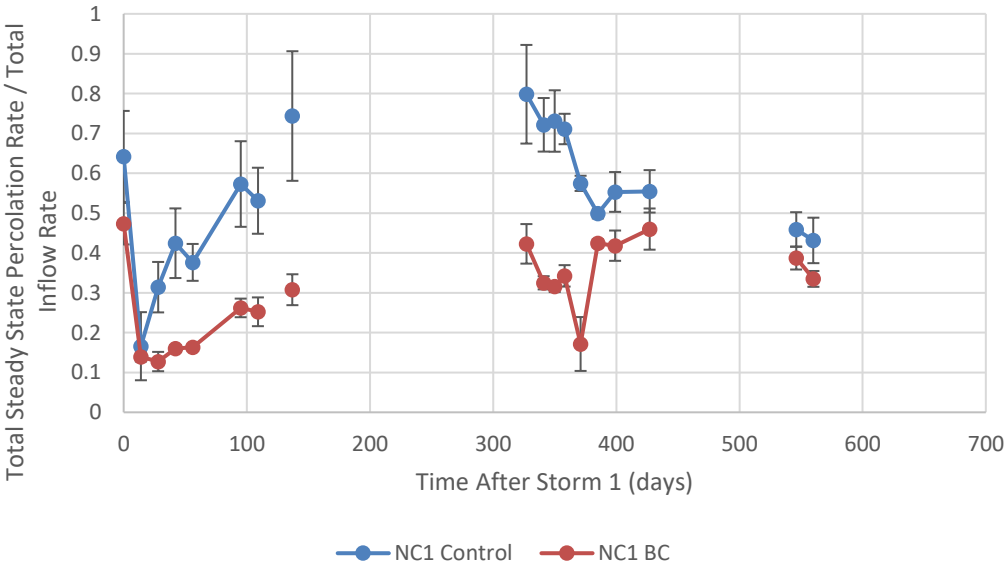

Figure A.9: Steady State percolation rate for NC-1 with error bars representing the standard error from three replicates.

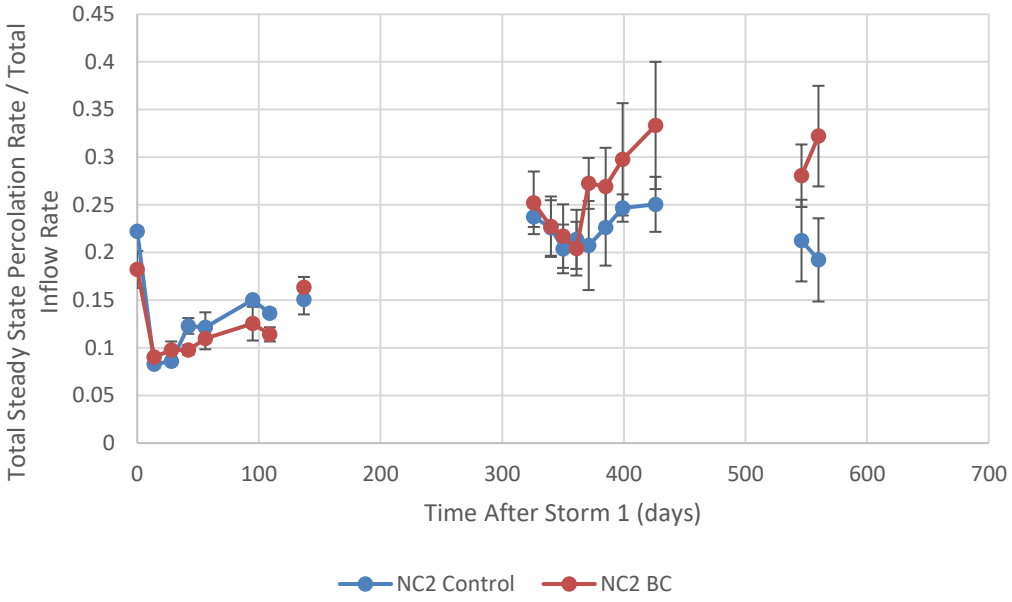

Figure A.10: Steady State percolation rate for NC-2 with error bars representing the standard error from three replicates.

Appendix B

Volumetric Water Content

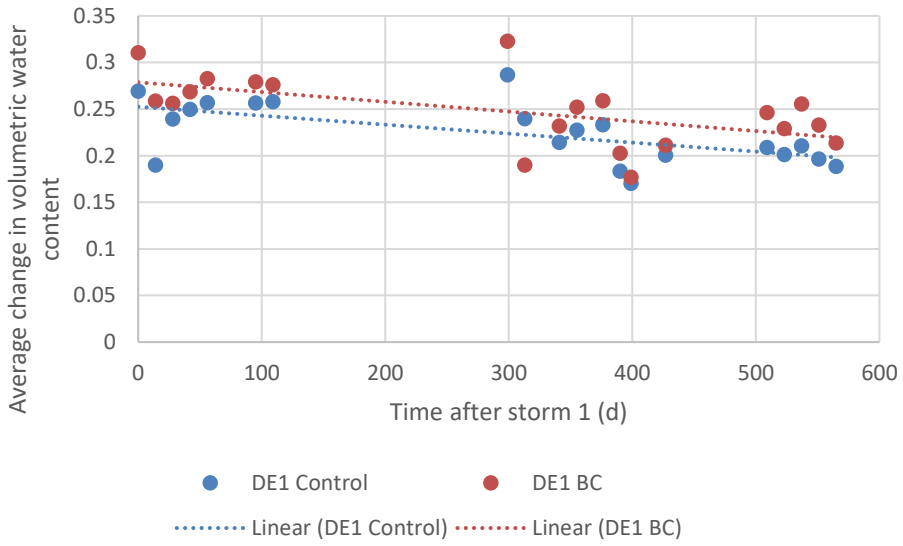

Figure B.1: Average change in volumetric water content versus time for DE-1.

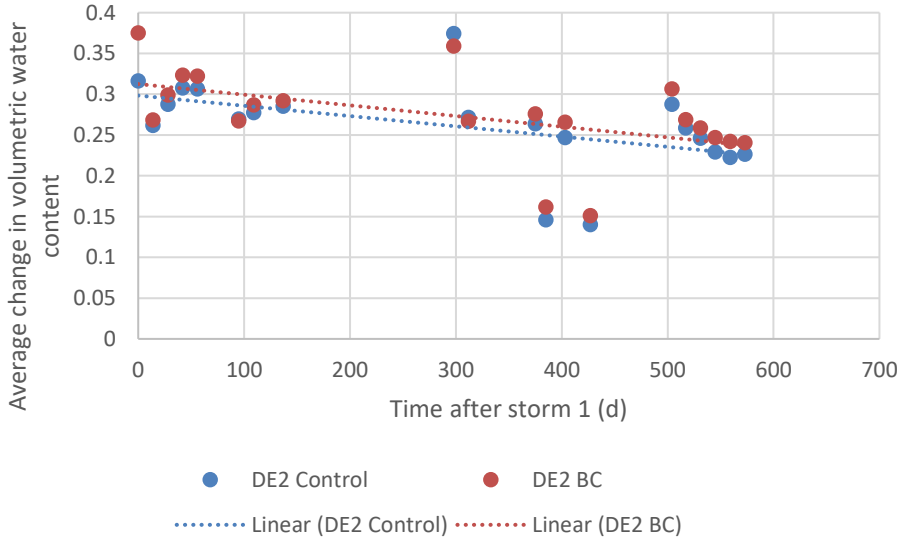

Figure B.2: Average change in volumetric water content versus time for DE-2.

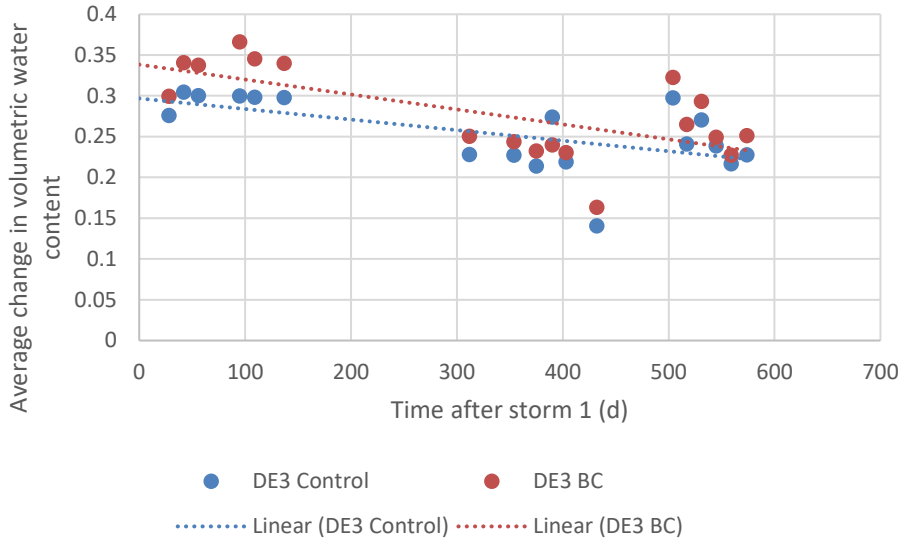

Figure B.3 Average change in volumetric water content versus time for DE-3.

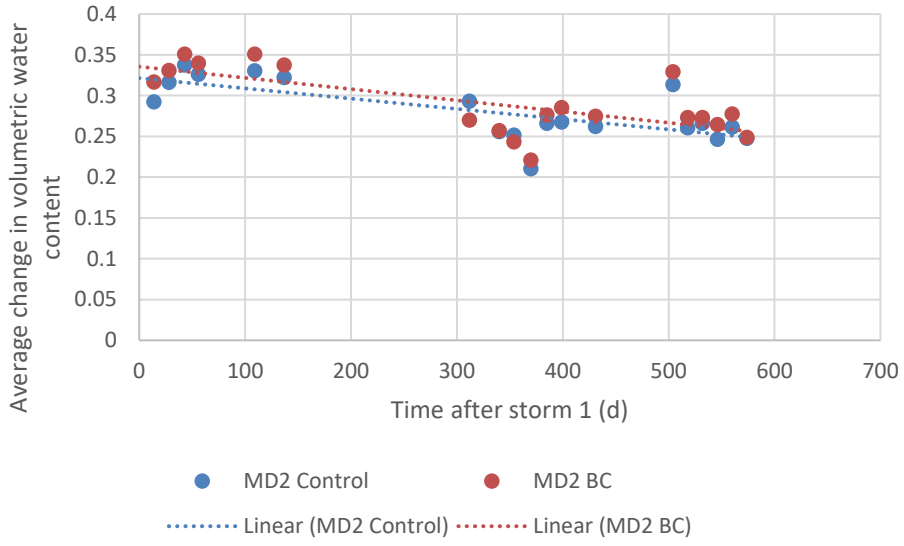

Figure B.4: Average change in volumetric water content versus time for MD-2.

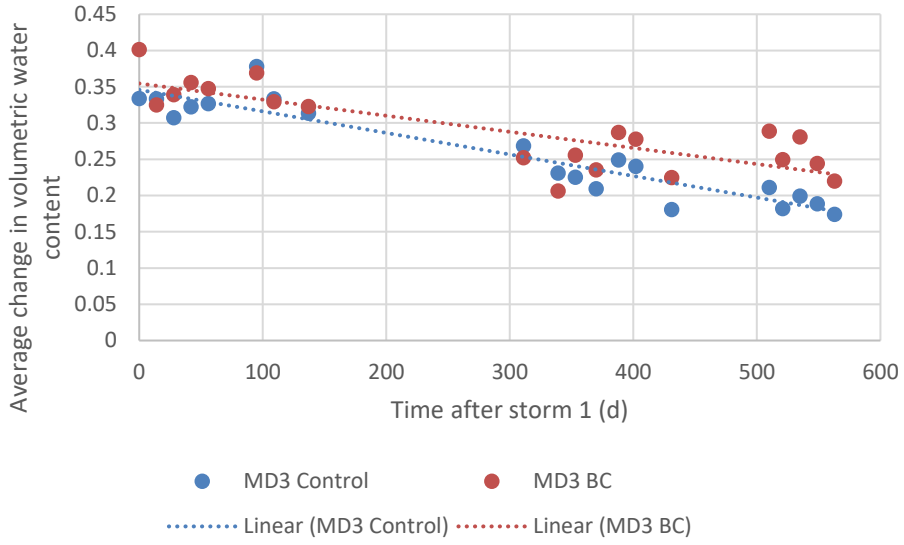

Figure B.5: Average change in volumetric water content versus time for MD-3.

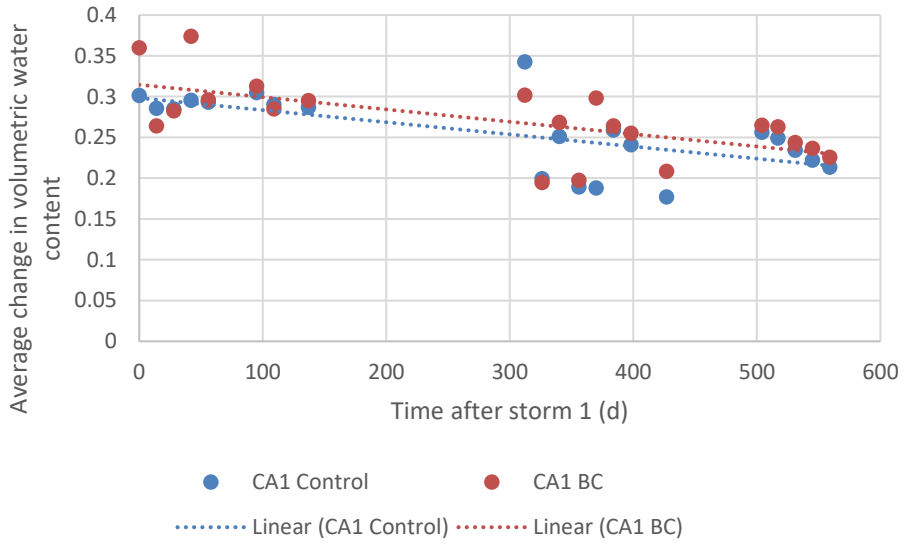

Figure B.6: Average change in volumetric water content versus time for CA-1.

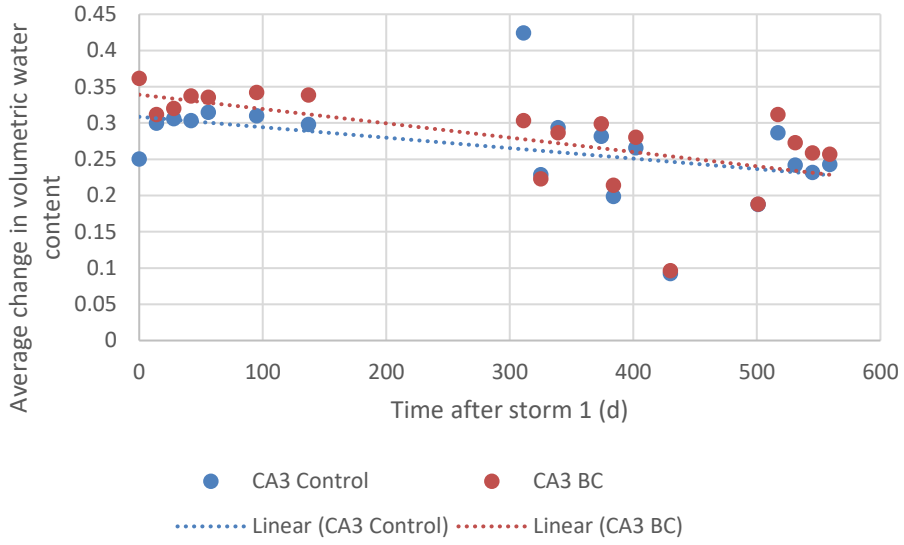

Figure B.7: Average change in volumetric water content versus time for CA-3.

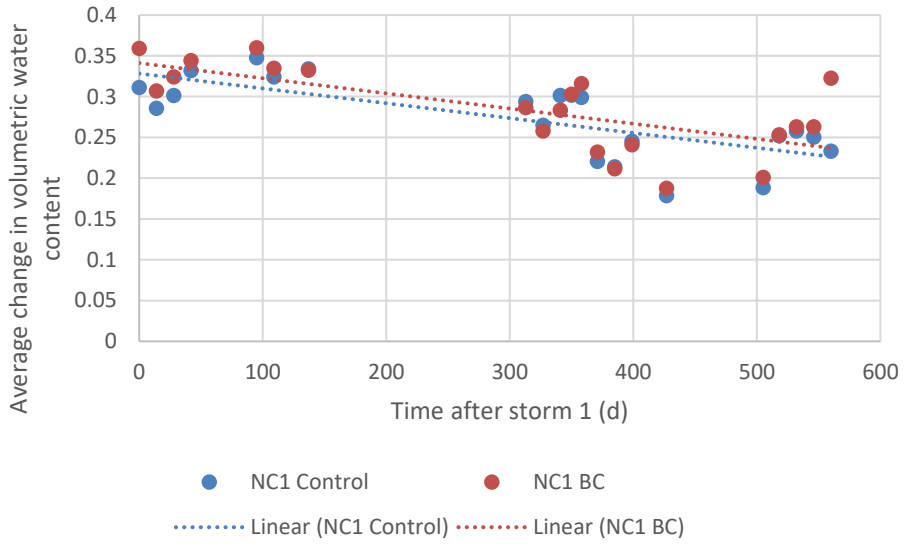

Figure B.8: Average change in volumetric water content versus time for NC-1.

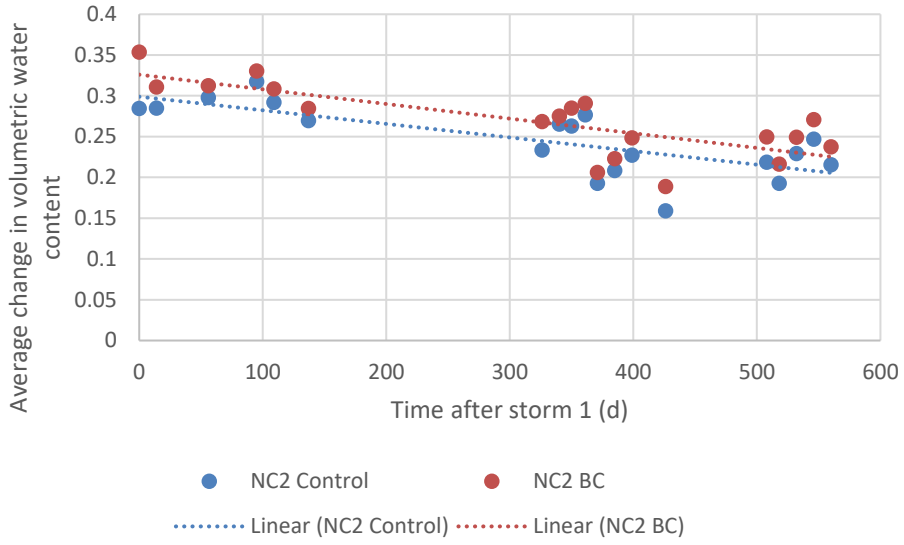

Figure B.9: Average change in volumetric water content versus time for NC-2.

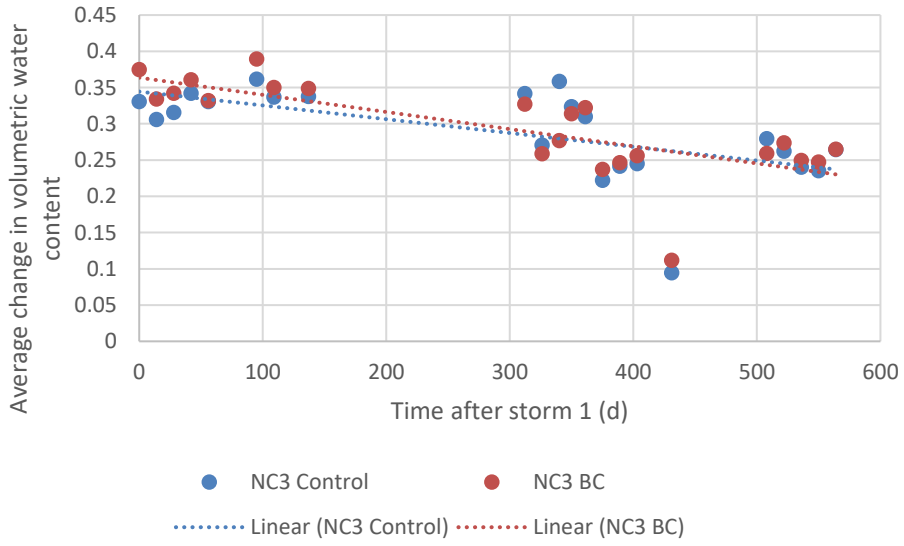

Figure B.10: Average change in volumetric water content versus time for NC-3.

Appendix C

Gravimetric Moisture Content Relations

C.1 Gravimetric Moisture Content and Soil Surface Cracking

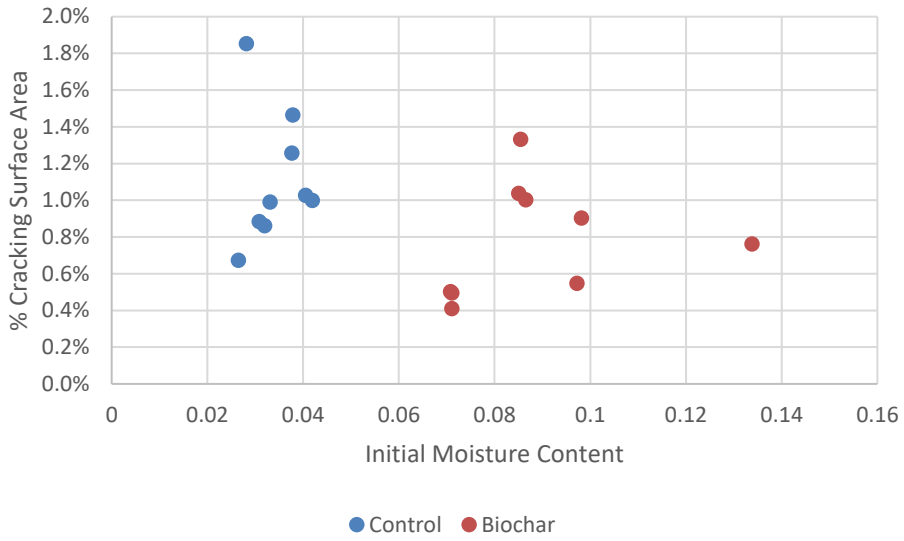

Figure C.1: Soil cracking surface area versus initial gravimetric moisture content for DE-1 in storms 23 through 25.

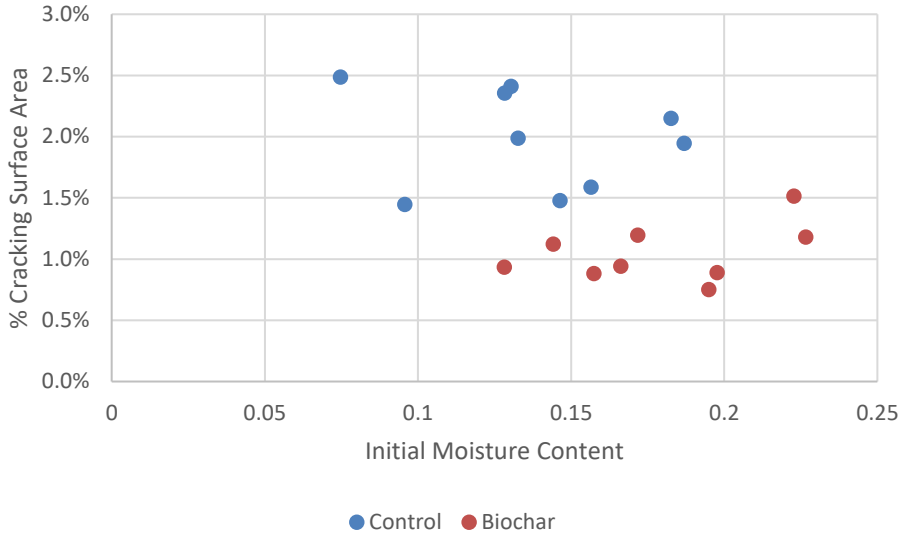

Figure C.2: Soil cracking surface area versus initial gravimetric moisture content for DE-3 in storms 23 through 25.

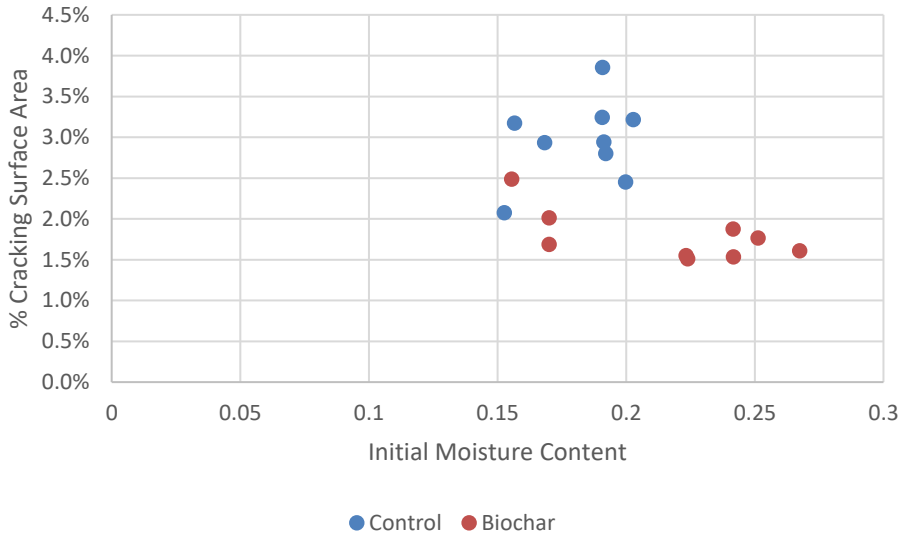

Figure C.3: Soil cracking surface area versus initial gravimetric moisture content for MD-1 in storms 23 through 25.

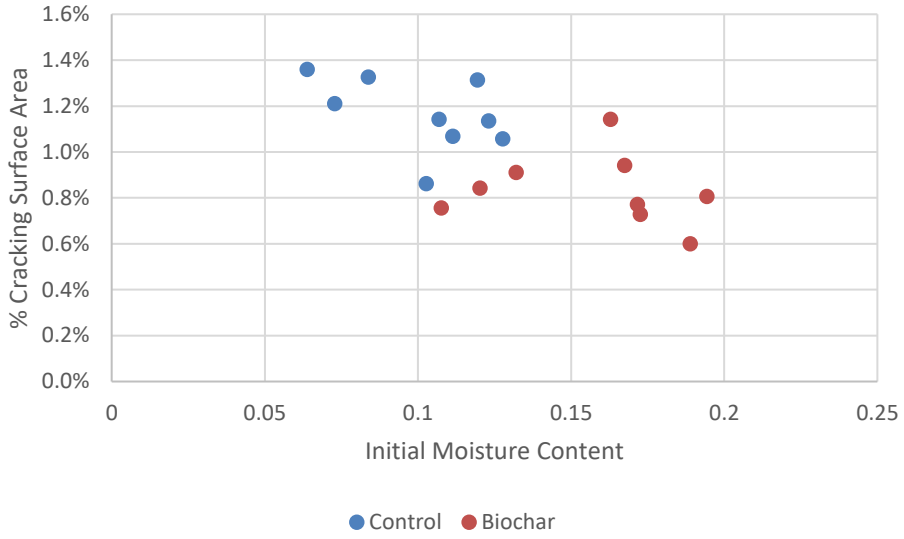

Figure C.4: Soil cracking surface area versus initial gravimetric moisture content for MD-2 in storms 23 through 25.

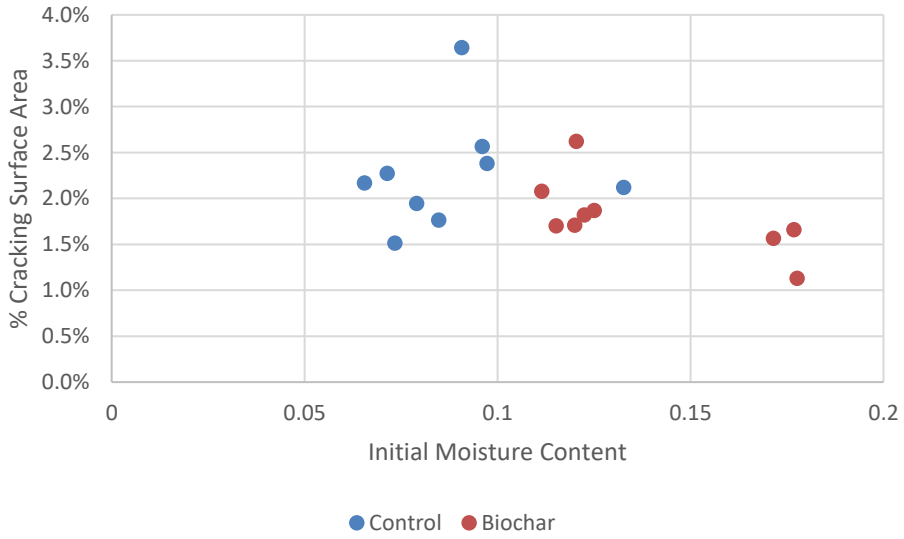

Figure C.5: Soil cracking surface area versus initial gravimetric moisture content for MD-3 in storms 23 through 25.

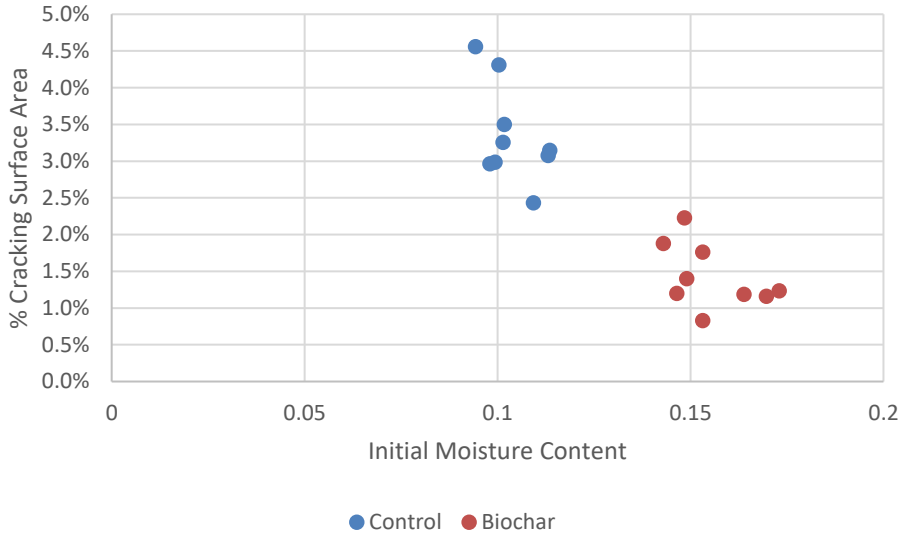

Figure C.6: Soil cracking surface area versus initial gravimetric moisture content for CA-1 in storms 23 through 25.

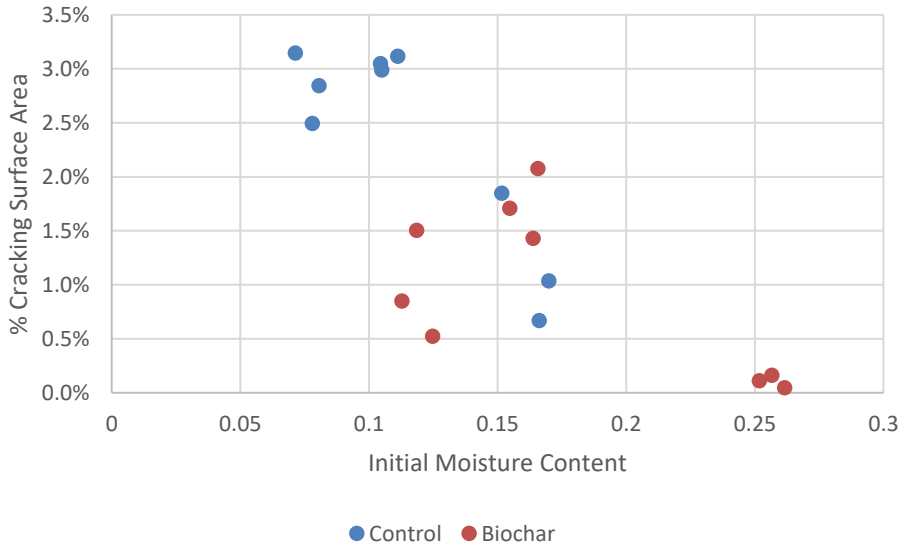

Figure C.7: Soil cracking surface area versus initial gravimetric moisture content for CA-3 in storms 23 through 25.

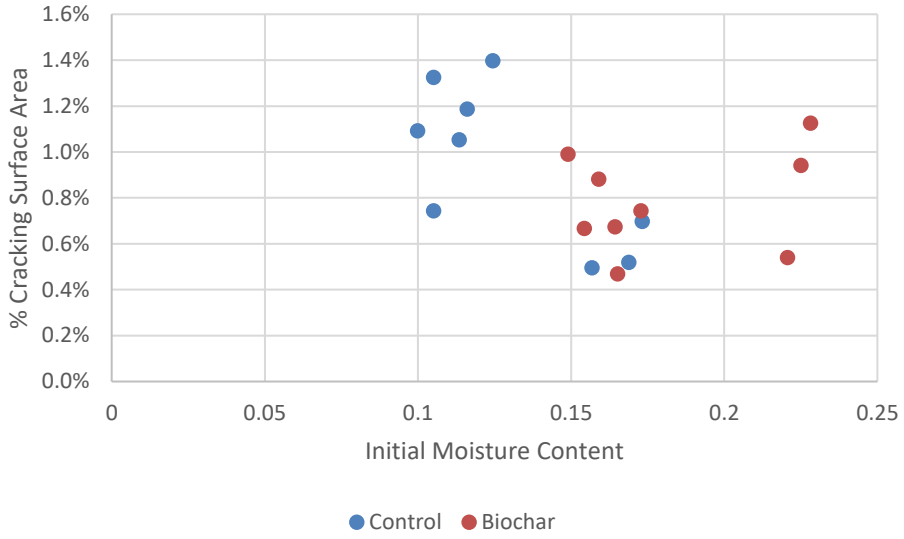

Figure C.8: Soil cracking surface area versus initial gravimetric moisture content for NC-1 in storms 23 through 25.

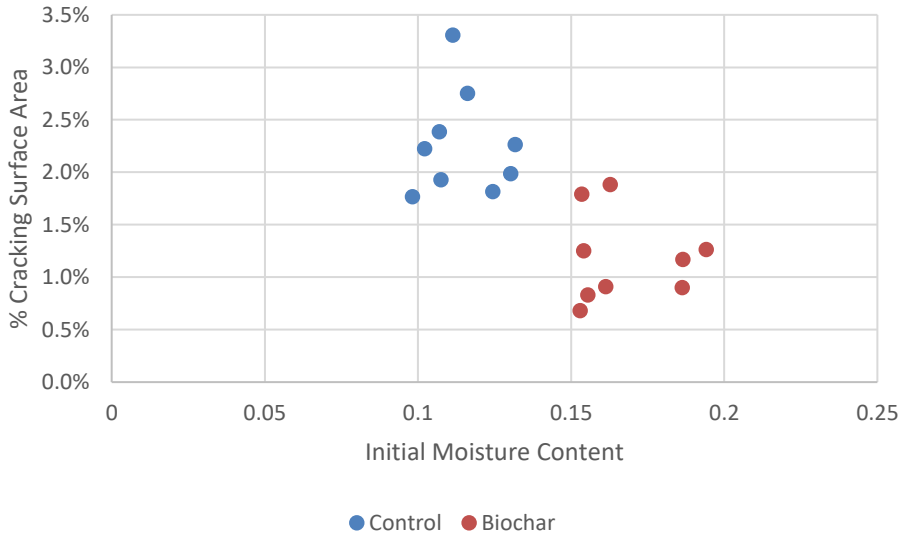

Figure C.9: Soil cracking surface area versus initial gravimetric moisture content for NC-2 in storms 23 through 25.

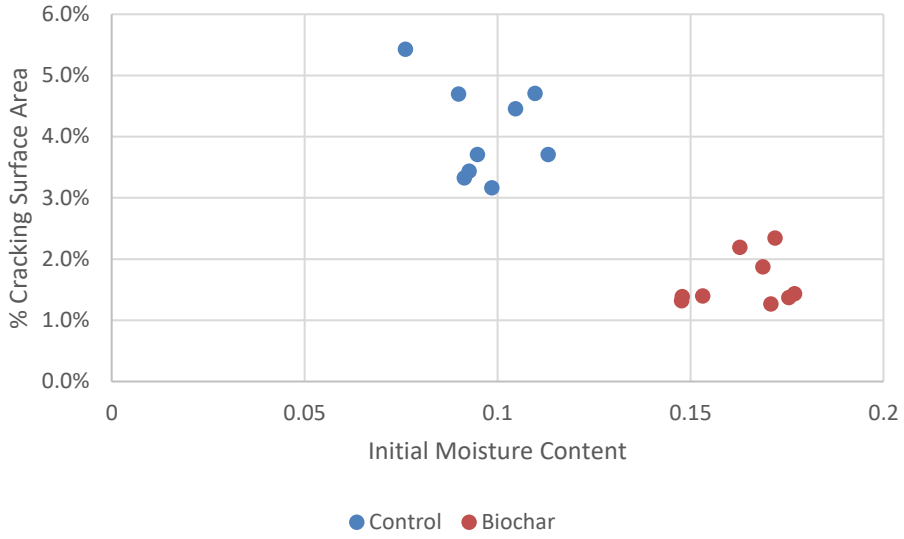

Figure C.10: Soil cracking surface area versus initial gravimetric moisture content for NC-3 in storms 23 through 25.

C.2 Gravimetric Moisture Content and Soil Volume

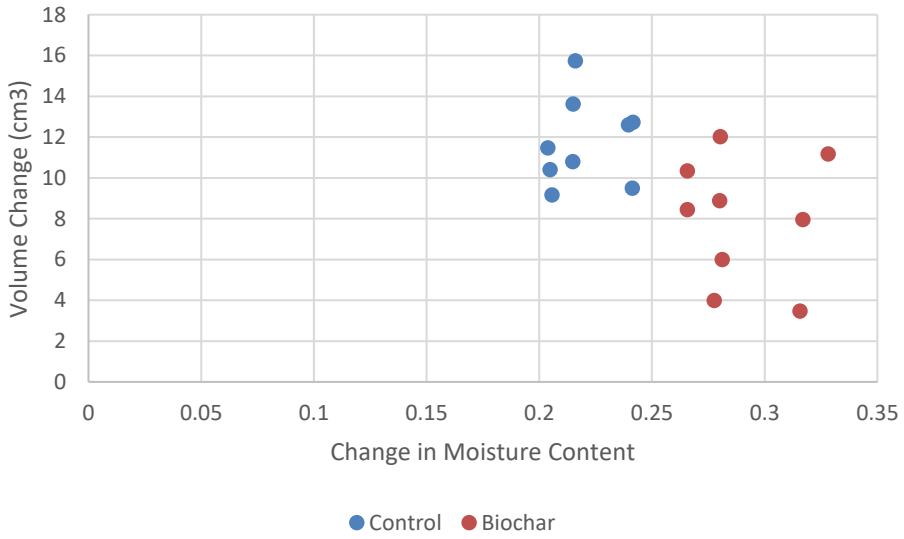

Figure C.11: Volume change versus change in gravimetric moisture content for DE-2 in storms 23 through 25.

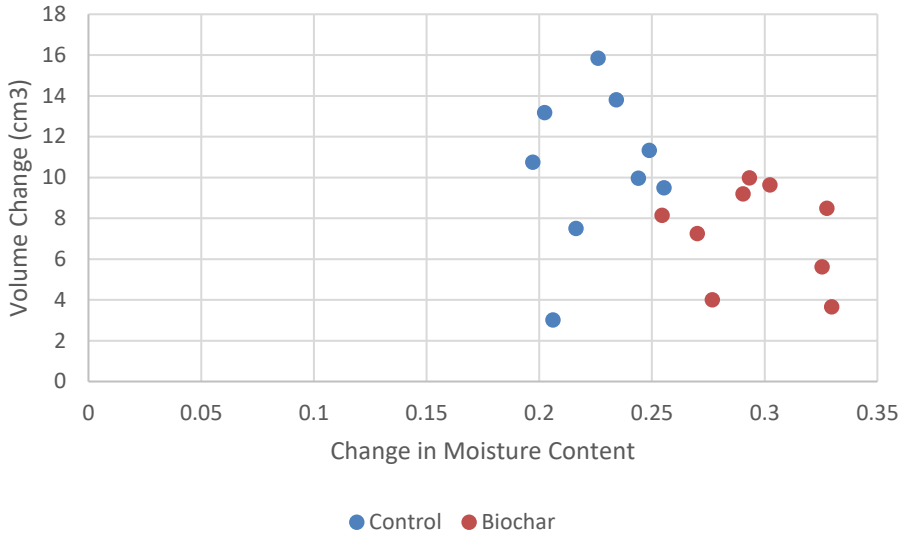

Figure C.12: Volume change versus change in gravimetric moisture content for DE-3 in storms 23 through 25.

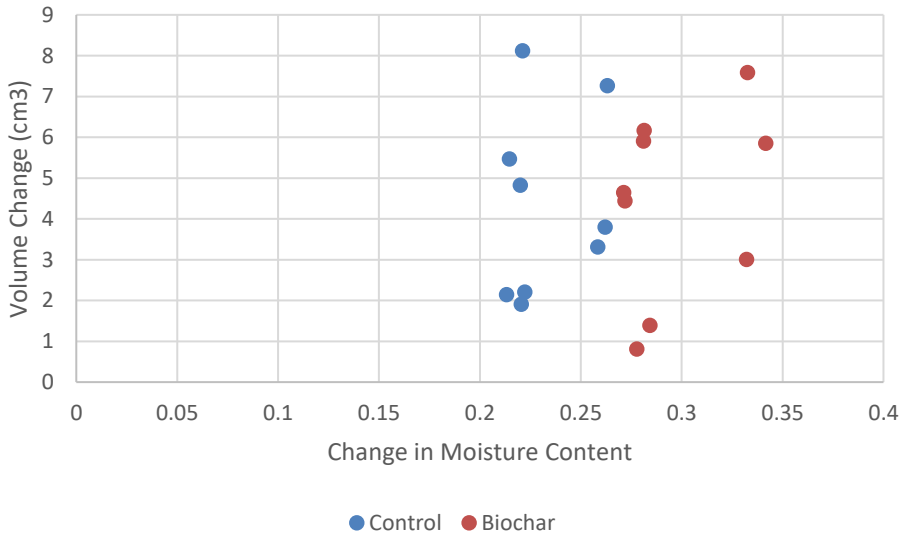

Figure C.13: Volume change versus change in gravimetric moisture content for MD-2 in storms 23 through 25.

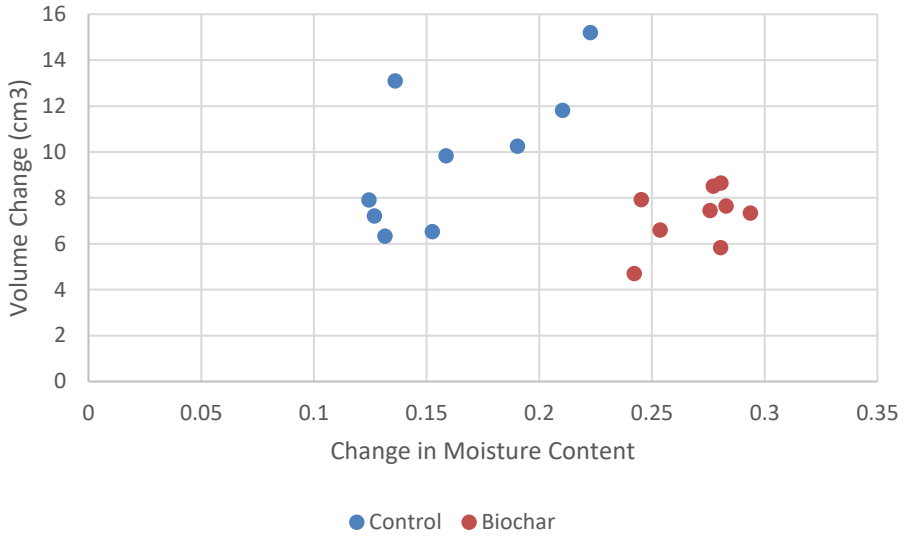

Figure C.14: Volume change versus change in gravimetric moisture content for MD-3 in storms 23 through 25.

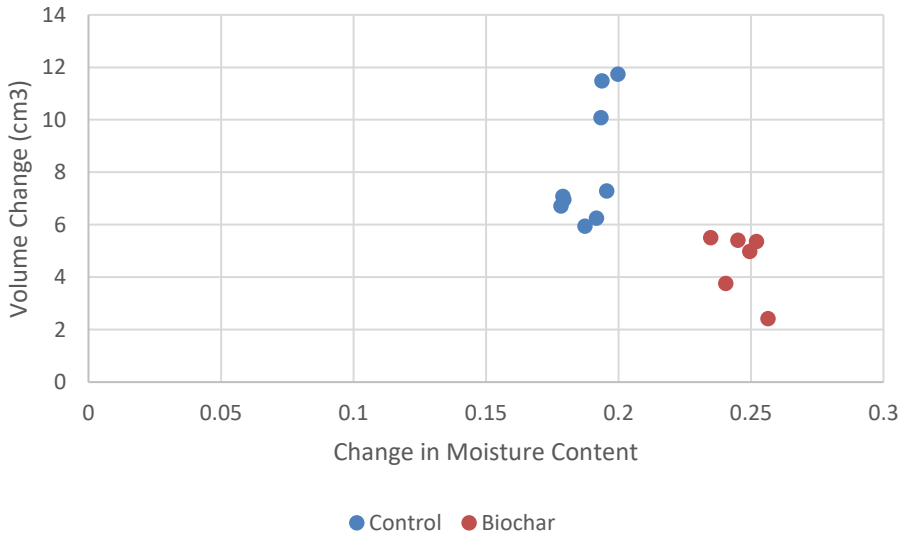

Figure C.15: Volume change versus change in gravimetric moisture content for CA-1 in storms 23 through 25.

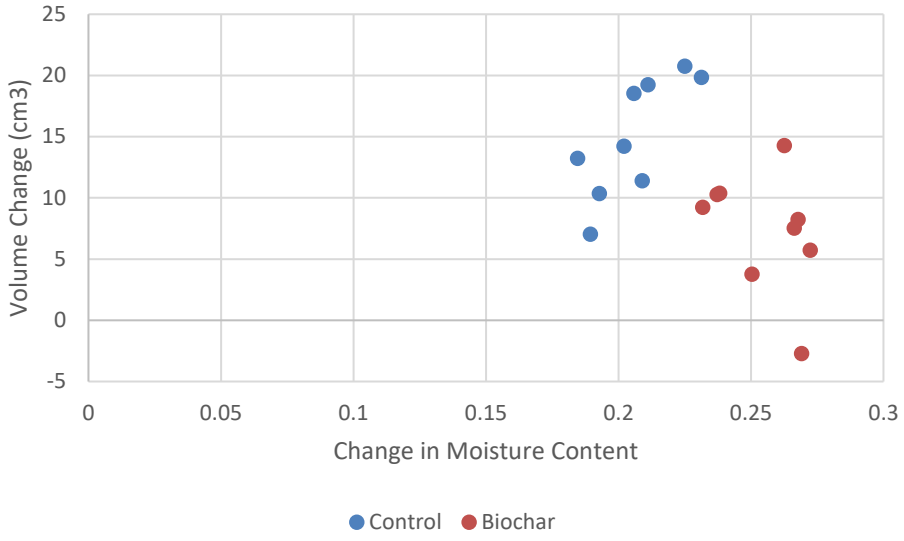

Figure C.16: Volume change versus change in gravimetric moisture content for CA-2 in storms 23 through 25.

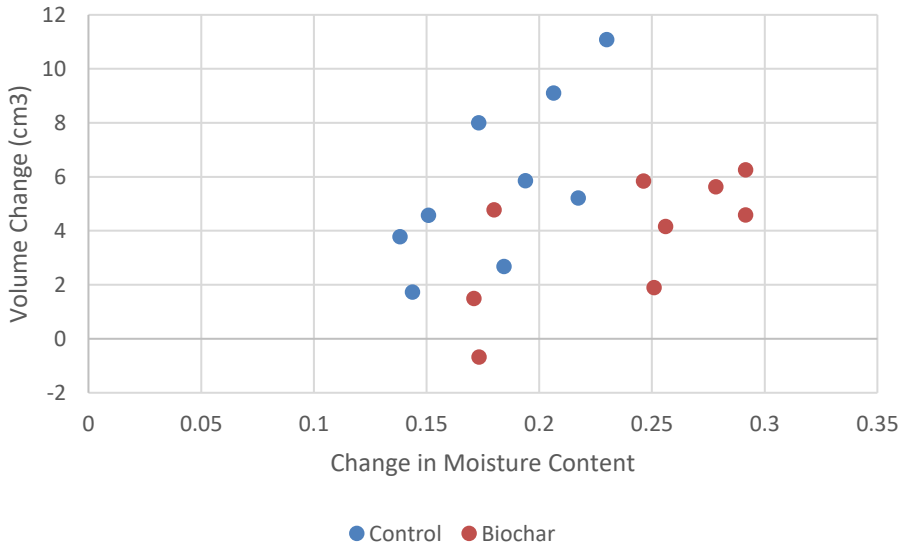

Figure C.17: Volume change versus change in gravimetric moisture content for CA-3 in storms 23 through 25.

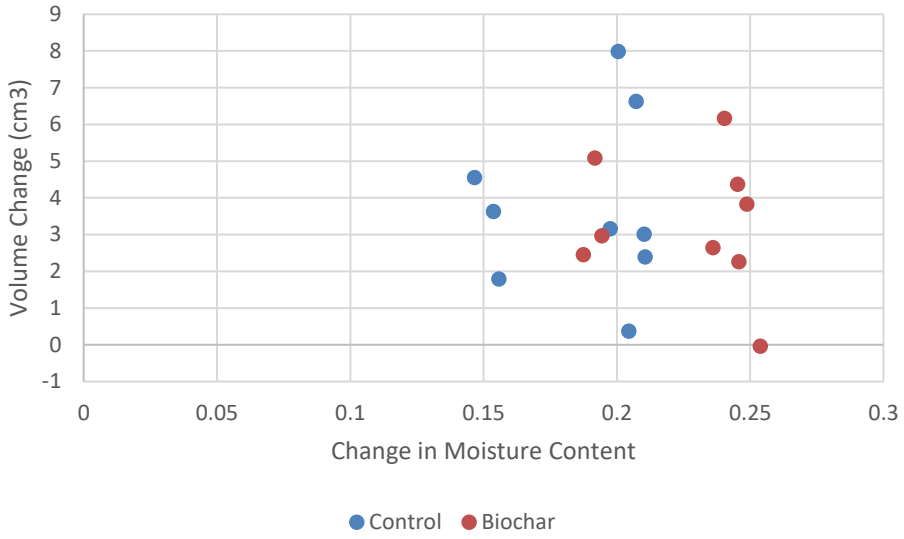

Figure C.18: Volume change versus change in gravimetric moisture content for NC-1 in storms 23 through 25.

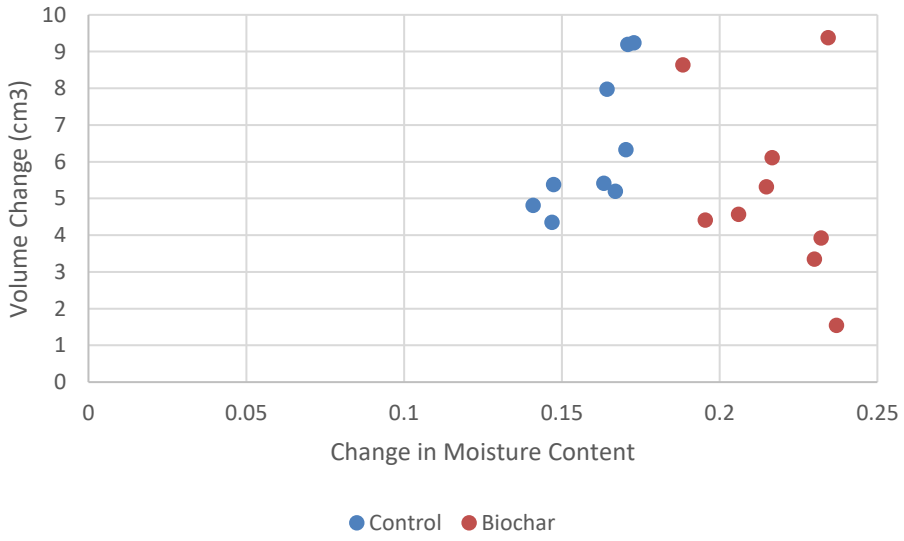

Figure C.19: Volume change versus change in gravimetric moisture content for NC-2 in storms 23 through 25.

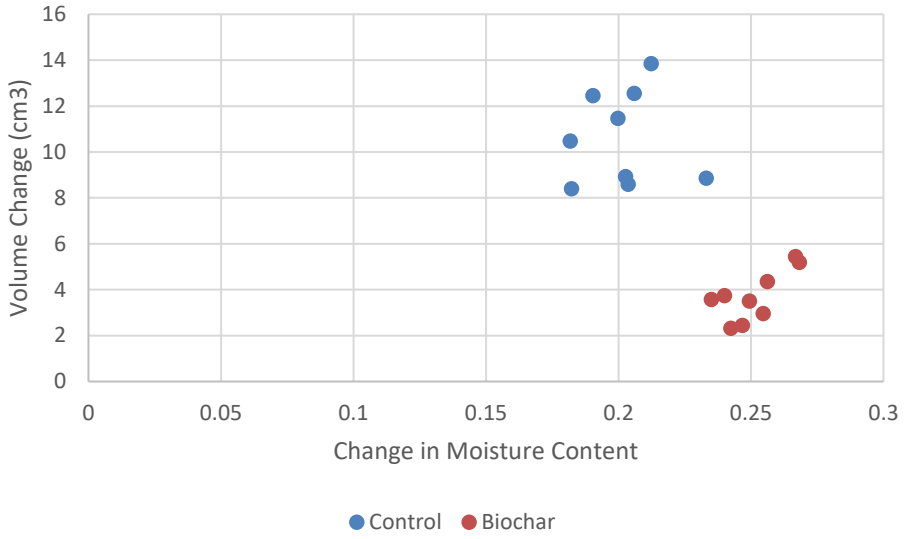

Figure C.20: Volume change versus change in gravimetric moisture content for NC-3 in storms 23 through 25.

Appendix D

Calendar

Table D.1: Timetable of Actions Performed

Activity	Date	Week
Reid: Column Packing	9/6/2019-9/25/2019	0
Reid: Columns Sealed Until All are Packed	9/6/2019-9/25/2019	0
Reid: Biweekly Storm Events	10/3/2019-12/7/2019	Week 1-10
Reid: Measurement of Percolation Rate	10/3/2019-12/7/2019	Week 1-10
Reid: Measurement of Effective Hydraulic Conductivity	10/3/2019-12/7/2019	Week 1-10
Reid: Measurement of Volumetric Water Content	10/3/2019-12/7/2019	Week 1-10
Reid: Columns Sealed for Holiday Break	12/7/2019-1/15/2020	Week 11-16
Reid: Biweekly Storm Events	1/6/2020-2/26/2020	Week 15-22
Reid: Measurement of Percolation Rate	1/6/2020-2/26/2020	Week 15-22
Reid: Measurement of Effective Hydraulic Conductivity	1/6/2020-2/26/2020	Week 15-22
Reid: Measurement of Volumetric Water Content	1/6/2020-2/26/2020	Week 15-22
Reid: Columns Sealed for COVID Closure	2/26/2020-7/14/2020	Week 22-42
Reid: Biweekly Storm Events	7/14/2020-9/29/2020	Week 42-53
Reid: Measurement of Effective Hydraulic Conductivity	7/14/2020-9/29/2020	Week 42-53

Reid: Measurement of Volumetric Water Content	7/14/2020-9/29/2020	Week 42-53
Reid: Measurement of Percolation Rate	7/14/2020-9/29/2020	Week 42-53
Brendan: Biweekly Storm Events	10/1/2020-11/17/2020	Week 53-60
Brendan: Measurement of Percolation Rate	10/1/2020-11/17/2020	Week 53-60
Brendan: Measurement of Effective Hydraulic Conductivity	10/1/2020-11/17/2020	Week 53-60
Brendan: Measurement of Volumetric Water content	10/1/2020-11/17/2020	Week 53-60
Brendan: Columns Sealed for Thanksgiving Break	11/17/2020-12/3/2020	Week 60-62
Brendan: Biweekly Storm Events	12/3/2020-12/15/2020	Week 62-64
Brendan: Measurement of Percolation Rate	12/3/2020-12/15/2020	Week 62-64
Brendan: Measurement of Effective Hydraulic Conductivity	12/3/2020-12/15/2020	Week 62-64
Brendan: Measurement of Volumetric Water Content	12/3/2020-12/15/2020	Week 62-64
Ali: Biweekly Storm Events	12/18/2020-1/7/2021	Week 64-67
Brendan: Biweekly Storm Events	1/9/2021-5/7/2021	Week 67-84
Brendan: Measurement of Volumetric Water Content	1/9/2021-5/7/2021	Week 67-84
Brendan: Measurement of Soil Surface Cracking	1/9/2021-5/7/2021	Week 67-84
Brendan: Measurement of Soil Volume	1/21/2021-5/7/2021	Week 69-84

Brendan: Measurement of Percolation Rate	4/1/2021-5/7/2021	Week 79-84
Brendan: Measurement of Saturated Hydraulic Conductivity	4/1/2021-5/7/2021	Week 79-84
Marcus: X-Ray Scanning of Columns	4/22/2021-5/7/2021	Week 82-84

Appendix E

Column Dimensions

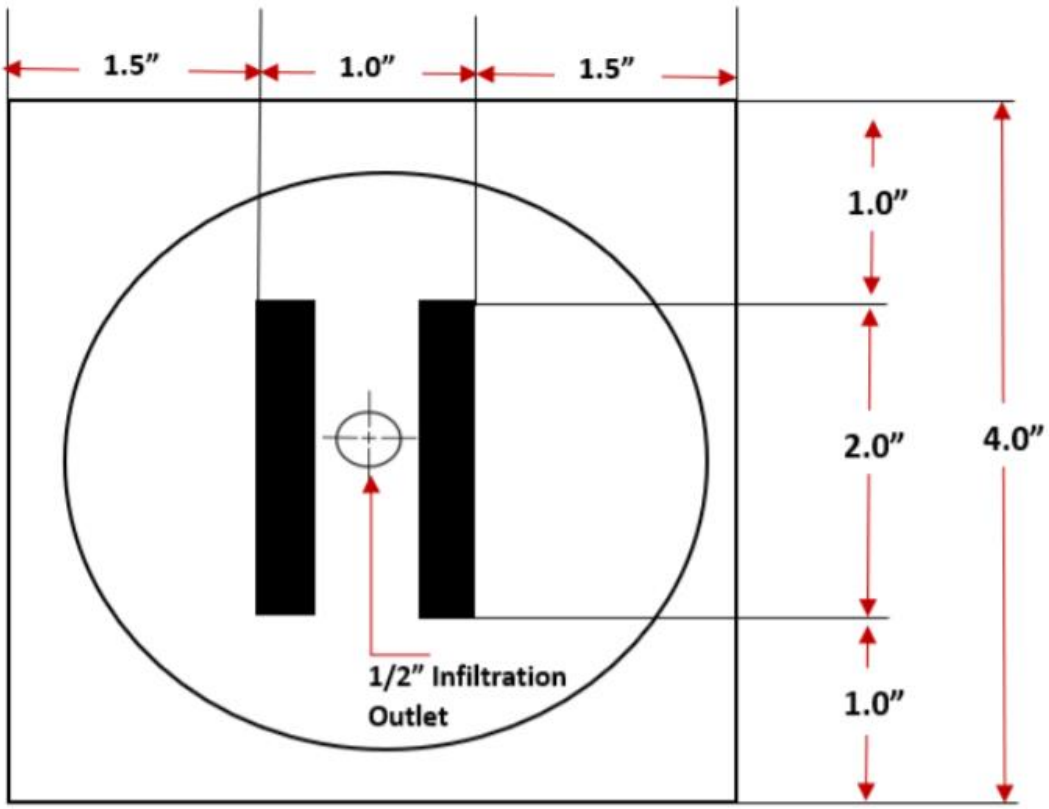

Figure E.1: Plan view of column dimensions (taken with permission from Reid, 2020).

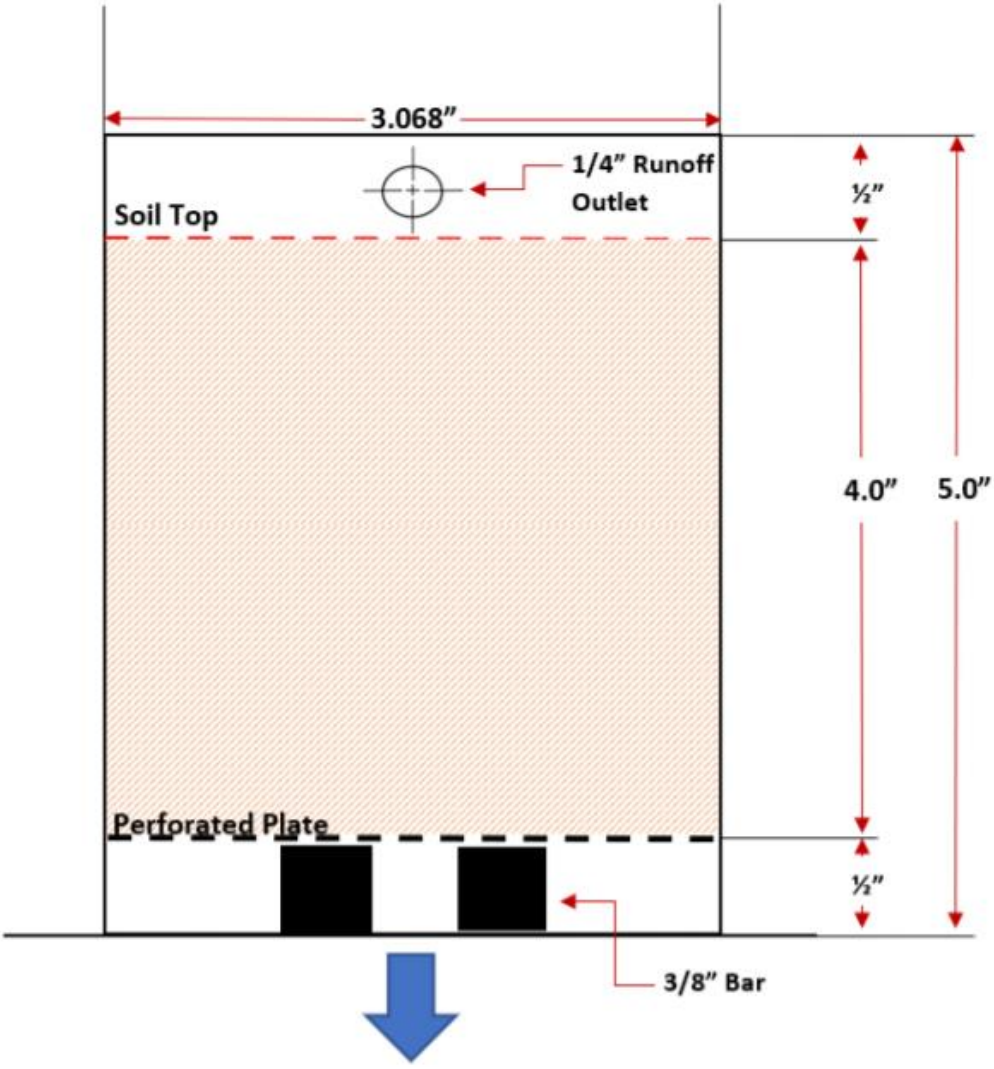

Figure E.2: Elevation view of column dimensions (taken with permission from Reid, 2020).